

## Do we really know the dust? Systematics and uncertainties of the mid-infrared spectral analysis methods

A. Juhász<sup>1</sup>, Th. Henning<sup>1,2</sup>, J. Bouwman<sup>1</sup>, C.P. Dullemond<sup>1</sup>, I. Pascucci<sup>3</sup>, D. Apai<sup>4,5</sup>

juhasz@mpia-hd.mpg.de

### ABSTRACT

The spectral region around  $10\ \mu\text{m}$ , showing prominent emission bands from various dust species is commonly used for the evaluation of the chemical composition of protoplanetary dust. Different analysis methods have been proposed for this purpose, but so far, no comparative test has been performed to test the validity of their assumptions. In this paper, we evaluate how good the various methods are in deriving the chemical composition of dust grains from infrared spectroscopy.

Synthetic spectra of disk models with different geometries and central sources were calculated, using a 2D radiative transfer code. These spectra were then fitted in a blind test by four spectral decomposition methods. We studied the effect of disk structure (flared vs. flat), inclination angle, size of an inner disk hole and stellar luminosity on the fitted chemical composition.

Our results show that the dust parameters obtained by all methods deviate systematically from the input data of the synthetic spectra. The dust composition fitted by the new two-layer temperature distribution method, described in this paper, differs the least from the input dust composition and the results show the weakest systematic effects. The reason for the deviations of the results given by the previously used methods lies in their simplifying assumptions. Due to the

---

<sup>1</sup>Max-Planck-Institut für Astronomie, Königstuhl 17, D-69117 Heidelberg, Germany

<sup>2</sup>Kavli Institute for Theoretical Physics, Kohn Hall, University of California, Santa Barbara, CA 93106, USA

<sup>3</sup>Johns Hopkins University, 3400 N. Charles St. Baltimore, MD 21218, USA

<sup>4</sup>Space Telescope Science Institute, 3700 San Martin Drive, Baltimore, MD 21218, USA

<sup>5</sup>Laplace Team of NASA Astrobiology Institute

radial extent of the  $10\ \mu\text{m}$  emitting region there is dust at different temperatures contributing to the flux in the silicate feature. Therefore, the assumption of a single averaged grain temperature can be a strong limitation of the previously used methods. The continuum below the feature can consist of multiple components (e.g., star, inner rim, disk midplane), which cannot simply be described by a Planck function at a single temperature. In addition, the optically thin emission of "featureless" grains (e.g., carbon in the considered wavelength range) produces a degeneracy in the models with the optically thick emission of the disk.

The effect of different noise levels on the results has also been tested. We find that for a signal-to-noise ratio of 100 one can expect an *absolute* uncertainty in the value of the crystallinity of about 11% using ground based observations ( $8\text{--}13\ \mu\text{m}$ ). For space based observations ( $7\text{--}17\ \mu\text{m}$ ) the expected uncertainty is about 5% for the same signal-to-noise value. Moreover, the average value of the estimated crystallinity increases toward lower signal-to-noise ratios in general. On the basis of our results, we propose a recipe for the analysis and interpretation of dust spectroscopy data in the mid-infrared which should be especially valuable for analyzing Spitzer spectroscopy data and ground-based infrared spectroscopy data in the  $10\ \mu\text{m}$  window.

*Subject headings:* astrochemistry – infrared:general – stars:circumstellar matter – protoplanetary disks – lines:profiles

## 1. Introduction

Excess emission above the stellar photosphere at mid-infrared wavelengths is a characteristic feature of Young Stellar Objects (YSOs). This infrared excess is caused by the thermal emission of circumstellar dust around the central star gathered in a disk-like structure and/or envelope. The amount of excess emission and the shape of the Spectral Energy Distribution (SED) is indicative of the evolutionary state of the object (e.g., van Boekel et al. 2006). Not only geometrical and density the structure of the circumstellar material, but also the dust properties evolve with time, due to, e.g., crystallization and coagulation (e.g., Beckwith et al. 2000; Henning et al. 2006 and references therein), vaporization and re-condensation (Gail 2004).

The dust evolution and grain processing can be even more clearly seen in the emission/absorption features observed in the mid-infrared spectrum of many young stars with a wide range of spectral types (e.g., Molster & Waters 2003; Apai et al. 2005; Bouwman et al. 2008; Henning 2008 (in press)). The most frequently observed features, around 10 and

18  $\mu\text{m}$ , are caused by amorphous and crystalline silicate grains. In the case of disk emission spectra, they arise from optically thin regions. Therefore, their shape is directly determined by the optical properties of the individual dust grains. The silicate features have been used in order to determine the dust properties, e.g., the fraction of crystalline grains, the iron/magnesium ratio or the characteristic grain size in surface layers of protoplanetary disks (e.g., Waelkens et al. 1996; Bouwman et al. 2001; Li et al. 2004; van Boekel et al. 2005b) or of Solar System comets (Crovisier et al. 1997; Brucato et al. 1999; Wooden 2002; Min et al. 2005b). Amorphous silicates with olivine and pyroxene stoichiometry are common materials in the diffuse interstellar medium (ISM) as well as in circumstellar disks (Henning et al. 2005). The broad and smooth features with a peak at approximately 9.7  $\mu\text{m}$  and 18.5  $\mu\text{m}$  are attributed to the Si–O stretching and O–Si–O bending modes, respectively, in amorphous silicate grains. Crystalline silicates (e.g., forsterite and enstatite) have in particular been observed in protoplanetary disks and they seem to be absent from the diffuse ISM. Kemper et al. (2005) placed an 2.2% upper limit for the crystallinity fraction of the silicates in the diffuse ISM. Thus it seems to be reasonable to conclude that crystalline silicates form in protoplanetary disks. However, the details of the formation process remain unclear. Crystalline silicate grains can be produced by direct condensation from the gas phase (Gail 2004) or by annealing of amorphous grains at higher temperatures (Fabian et al. 2000; Gail 2001; Harker & Desch 2002), or both processes.

Space-based observations of disks with the *Infrared Space Observatory* (ISO) and the *Spitzer Space Telescope* (SST) as well as ground-based measurements with, e.g., TIMMI2, TReCS or COMICS, enabled the detailed investigation of the silicate features. Such studies have shown that dust processing clearly occurs in protoplanetary disks around stars with different spectral types (e.g., Bouwman et al. 2001; van Boekel et al. 2005b; Apai et al. 2005; Kessler-Silacci et al. 2006; Honda et al. 2006; Sargent et al. 2006; Watson et al. 2007; Sicilia-Aguilar et al. 2007; Bouwman et al. 2008). These studies also demonstrated that evidence for grain growth can be found in the mid-infrared spectra, indicated by the broadening of the 10  $\mu\text{m}$  emission feature together with a decrease of its height above the underlying continuum. The relation, however, between grain growth and crystallization and the role of the stellar type is a topic of ongoing debate. There are reports on possible correlations between grain growth and crystallization (van Boekel et al. 2005b; Apai et al. 2005; Kessler-Silacci et al. 2006) and on an inverse correlation between the average grain size and stellar type (Kessler-Silacci et al. 2006) and a possible inverse correlation between the crystallinity and the stellar temperature (Apai et al. 2005).

The results of these studies depend not only on the quality of observational data, but also on the applied analytical methods. Here, we should also note, that the features are produced in the surface layer and the material properties are not necessary typical of the

material in the disk midplane. In addition, the region emitting the  $10\ \mu\text{m}$  feature will be located at different distances from the central star, depending on the radiation characteristics of the star and the nature of the dust grains and the disk properties. Due to the lack of a comparative study of the various analysis methods, it is practically impossible to find out if the relations, discussed above, are really present or if they are caused by systematic uncertainties in the applied methods. Since we can determine the physical properties and chemical composition of protoplanetary dust grains for a larger sample only via such spectral decomposition methods, it is important to know how good these methods are and which of them should be applied in a specific case. In this paper, using a 2D radiative transfer model of protoplanetary disks with a prescribed dust composition, we synthesize "observations" which we fit with three widely used spectral decomposition methods. We then compare the resulting dust composition to the original input composition. We also propose a new and fast method for fitting the mid-infrared spectral features in which we apply a distribution of temperatures, leading to more reliable results.

## 2. Modelling

### 2.1. Disk models

In order to investigate the quality of the spectral decomposition methods, we fitted synthetic spectra calculated by the 2D radiative transfer code RADMC (Dullemond & Dominik 2004). Although this code assumes an axisymmetric density distribution, photon packages are followed in three dimensions by a Monte Carlo method. After the temperature distribution has been determined, the ray tracing module of the more general code RADICAL (Dullemond & Turolla 2000) has been used to compute the SEDs. These codes have already been used to model protoplanetary disk SEDs in numerous studies (Pontoppidan & Dullemond 2005; van Boekel et al. 2005a; Dullemond & Dominik 2004) and tested against other continuum radiative transfer codes (Pascucci et al. 2004).

The disk structure can possibly be related to grain evolution. A flared disk, containing unprocessed, small amorphous grains becomes flattened with time as dust grains grow and settle to the disk midplane (Bouwman et al. 2008). Since the flaring angle of the disk has a strong effect on the shape of the continuum at mid-infrared wavelengths (Dullemond & Dominik 2004), it can also have an effect on the results of the spectral analysis methods. Therefore, we used disk models with different geometries. We want to note that we did not treat the dust coagulation and sedimentation in a self-consistent way during the modelling. Since the irradiated area of a circumstellar disk depends on the luminosity of the central star, we used stars with three different types (Herbig Ae star, T Tauri star and

Brown Dwarf) as central radiation source in our models. The main parameters of the 2D RT disk models as well as the applied stellar properties are summarized in Tab. 1. The stellar emission has been modelled by a blackbody radiation source instead of a Kurucz model (Kurucz 1993), which made the models more uniform enabling us to compare the results directly.

We calculated six series of disk models in order to investigate the effect of disk structure and disk orientation on the results of the fitting procedure. Each of the model series contained 12 spectra: three different stellar types and four different inclinations from pole-on to close to edge-on orientation ( $0^\circ$ ,  $20^\circ$ ,  $45^\circ$ ,  $70^\circ$ ). The mass of the disk in each model has been scaled with the stellar mass as  $M_{\text{disk}} = 0.03M_\star$ . The surface density as a function of radius was described by a power law as  $\Sigma(r) = \Sigma_0(r/r_{\text{disk}})^p$ , where  $\Sigma_0$  is the surface density at the outer disk radius and  $p = -1$ . The outer radius of the Herbig Ae disk was set to 400 AU. Then the outer disk radius of the T Tauri and Brown Dwarf disks was determined by the radial optical depth at  $0.55 \mu\text{m}$ , which we took to be same as in the Herbig Ae disk. It is important to note that the chemical composition of dust grains was assumed to be uniform throughout the disk. This simplifying assumption will be less justified when considering a large wavelength range and, therefore, a wider temperature and radial region in the disk. The passive irradiated disk model of Dullemond et al. (2001) has been applied for the disk structure in general, but the detailed structure of the disks were different in the different model series. The six model series can be summarized as follows.

**Model AS, AB.** A flared disk geometry has been applied with a flaring index  $\alpha$  (see Eq. A3) of  $2/7$  and with a dimensionless pressure scale height at the inner radius of  $H(R_{in})/R_{in} = 0.03$  (see Appendix A). The inner disk radius was determined by the sublimation temperature of 1500 K (Model AS) and 1060 K (Model AB). The models with 1060 K temperature at their inner edge have twice as large inner holes as the models with 1500 K temperature.

**Model BS, BB.** Here we applied a moderately flared disk with a flare index of  $1/7$  and with a dimensionless pressure scale height at the inner radius of  $H(R_{in})/R_{in} = 0.03$ . The inner disk radius is again determined by the grain temperature of 1500 K (Model BS) and 1060 K (Model BB).

**Model CS, CB.** A more flattened disk model has been considered here compared to the Model B series. We used a similar density structure for these models as it was used for Model B disks. For Model C the flaring index was set to  $1/8$  producing a self-shadowed flattened disk structure. The inner disk radius was again set by the grain temperature of 1500 K (Model CS) and 1060 K (Model CB).

## 2.2. Mass absorption coefficients

During the tests, we used six different dust species (amorphous silicates with olivine and pyroxene stoichiometry, forsterite, enstatite, silica and carbon), each with three grain sizes (0.1, 1.5 and 6.0  $\mu\text{m}$ ). Tab. 2 summarizes the used dust species, grain model and origin of the optical constants. The relative mass fraction for each dust species and grain size used in the study is presented in Tab. 3. The used relative mass fractions as a function of grain size corresponds to number density distribution of  $n \propto a^{-3.5}$  and  $n \propto a^{-3.3}$  for the amorphous and crystalline dust species, respectively. The mass absorption coefficients of these dust species as a function of wavelength are shown in Fig. 1. In order to calculate the mass absorption coefficient from the optical constants, we used the theory of Distribution of Hollow Spheres (DHS) (Min et al. 2005a) for crystalline silicates, while classical Mie theory for spherical particles was used for the amorphous dust species.

There are two distinct, but coupled problems related to the fitting of the mid-infrared silicate features. One of the problems is the applicability of a special set of optical data and the other one is the uncertainty in the applied spectral decomposition methods, themselves. It is unknown whether or not we use exactly the right optical data, which determine how the protoplanetary dust grains interact with radiation. The question of how good our set of mass absorption coefficients is is beyond the scope of this paper. Here, we used the same dust composition for all disk models (see Tab. 3), in order to evaluate the performance of the various spectral decomposition methods. We are aware that the use of one specific dust composition in all disk models is a limitation of the study, but it is impractical to test the methods on all possible combinations of dust mixtures and stellar/disk parameters. We chose, therefore, a single dust composition for the disk models the calculated spectra of which resembles that of typically seen towards young stellar objects. In this study we investigate how the different stellar and disk parameters can modify the results of spectral decomposition. The best way to isolate these effects is to use one dust mixture in all disk models, thus any difference between the input and the resulting dust parameters is certainly caused by the effects of stellar or disk parameters, which is then a deficiency of the applied method.

## 2.3. Fitting methods

Numerous techniques have been applied for the spectral decomposition of mid-infrared silicate features (e.g., Bouwman et al. 2001; Li et al. 2004; van Boekel et al. 2005b; Kessler-Silacci et al. 2006; Watson et al. 2007; Bouwman et al. 2008), but no systematic comparison of various techniques has been performed so far, leaving uncertainties in the quality and applicability

of these techniques. We choose the three most widely used methods and tested them against a new method described in this paper and applied them to the synthetic spectra of the above described disk models. These three methods have been applied by many authors to evaluate the chemical composition of protoplanetary dust from mid-infrared silicate features for a wide range of source types (e.g., Bouwman et al. 2001; Meeus et al. 2003; van Boekel et al. 2005b; Apai et al. 2005; Honda et al. 2006; Schegerer et al. 2006; Kessler-Silacci et al. 2006; Sicilia-Aguilar et al. 2007; Bouwman et al. 2008). All methods assume that the silicate emission comes from an optically thin region, but the temperature structure and underlying continuum is described in different ways in the distinct methods.

The simplest method for the spectral decomposition of the silicate emission feature is a continuum subtraction (hereafter COS) method (e.g., Bouwman et al. 2001). In this approach the continuum is fitted by a polynomial (usually first or second order) outside the feature and then subtracted from the spectrum. In the 5–36  $\mu\text{m}$  domain (*Spitzer* IRS) there are three possible wavelength ranges in which the continuum can be fitted; shortward of 7.5  $\mu\text{m}$ , between 12 and 15  $\mu\text{m}$  and longward of 30  $\mu\text{m}$ . The wavelength domains for the continuum fitting are not strictly determined. In this study we chose the following domains for the continuum fitting 6.8–7.5  $\mu\text{m}$ , 12.5–13.5  $\mu\text{m}$  and 30–36  $\mu\text{m}$ . A reasonable way to subtract the continuum has been developed by van Boekel et al. (2005b). Here the subtracted *and* normalized flux is given by

$$F_{\nu}^{\text{norm}} = 1 + \frac{F_{\nu} - F_{\nu}^{\text{cont}}}{\langle F_{\nu}^{\text{cont}} \rangle}. \quad (1)$$

Here,  $F_{\nu}$  is the flux density of the measured spectrum,  $F_{\nu}^{\text{cont}}$  is the flux density of the fitted continuum and  $\langle F_{\nu}^{\text{cont}} \rangle$  is the average value of the continuum flux density over all the frequencies in the fitted domain. For the spectral decomposition problem one can write

$$F_{\nu}^{\text{norm}} = \sum_{i=1}^N \sum_{j=1}^M C_{i,j} \kappa_{i,j}^{\text{norm}}, \quad (2)$$

where  $N$  is the number of dust species and  $M$  is the number of different grain sizes,  $\kappa_{i,j}^{\text{norm}}$  is the normalized mass absorption coefficient of the dust species  $i$  and grain size  $j$ . The mass fraction of a specific dust species can be calculated from the  $C_{i,j}$  values as

$$m_{i,j} = \frac{C_{i,j}}{\sum_{i=1}^N \sum_{j=1}^M C_{i,j}}. \quad (3)$$

The mass absorption coefficients should be normalized exactly the same way as it has been performed for the observed spectrum. In this fitting approach  $\kappa_{i,j}$  is given, while  $C_{i,j}$  has to be fitted.

A further step was taken by adopting a single black body function as the continuum. In this single-temperature (hereafter ST) approach (e.g., van Boekel et al. 2005b) the continuum and spectral features are fitted simultaneously and the observed flux density at a specific frequency is given by

$$F_\nu = C_0 B_\nu(T) + \sum_{i=1}^N \sum_{j=1}^M C_{i,j} B_\nu(T) \kappa_{i,j}. \quad (4)$$

Here  $\kappa_{i,j}$  is the mass absorption coefficient of the dust species  $j$  and the grain size  $i$ ,  $T$  is the temperature in the continuum *and* in the feature.  $B_\nu(T)$  is the Planck function at a temperature  $T$ , the quantities  $N$  and  $M$  denote the total number of different dust species and grain sizes, respectively. The mass fraction of a specific dust species is given by Eq. 3. In this spectral decomposition problem  $\kappa_{i,j}$  is given, while  $T$ ,  $C_0$  and  $C_{i,j}$  have to be fitted. An obvious limitation of this method is its simplistic treatment of the temperature structure of the radiating dust.

The subsequent evolution in data quality allowed the adoption of more realistic models to fit the  $10\ \mu\text{m}$  silicate feature. By fitting the continuum and the feature temperature in Eq. 4. separately one can obtain a more proper analyzing method. In this two-temperature (hereafter TT) approach (Bouwman et al. 2008) the flux density is given by

$$F_\nu = C_0 B_\nu(T_c) + \sum_{i=1}^N \sum_{j=1}^M C_{i,j} B_\nu(T_f) \kappa_{i,j}. \quad (5)$$

Here  $T_c$  is the temperature in the continuum and  $T_f$  is the temperature in the feature. In all the COS, ST and TT methods, we used a generalized version of the non-negative least-square optimization routine of Lawson & Hanson (1974). For the ST and TT methods a grid of temperatures was created first. Then the optimization routine evaluated the best fitting chemical composition for each temperature. During the tests the temperature step size was 10 K in the feature and 15 K in the continuum. The minimum and maximum temperatures in the continuum was 20 K and 4000 K, respectively. For the feature we used 20 K and 1500 K as the lowest and highest temperature, respectively. We assumed that dust grains evaporate at higher temperatures, while the lowest temperature was set to the temperature of the interstellar dust. In order to characterize the quality of the fit, we calculated the  $\chi^2$  value for each temperature, with

$$\chi^2 = \frac{1}{N_\nu - f} \sum_{i=1}^{N_\nu} \frac{(F_\nu^{\text{model}} - F_\nu^{\text{observed}})^2}{(F_\nu^{\text{error}})^2}. \quad (6)$$

Here  $N_\nu$  is the number of frequencies or wavelengths and  $f$  is the number of fitted parameters.  $F_\nu^{\text{observed}}$  is the flux density calculated by the 2D RT code,  $F_\nu^{\text{model}}$  is the fitted flux density



by the spectral decomposition method, and  $F_\nu^{\text{error}}$  is the uncertainty in  $F_\nu^{\text{observed}}$  and not the uncertainty of the 2D RT calculation. We simulated observations by calculating synthetic spectra and we used simulated observational flux uncertainties by  $F_\nu^{\text{error}} = 0.001 \cdot F_\nu^{\text{observed}}$ . Then the best fit chemical composition was the model, which had the lowest  $\chi^2$  value. Except for Sec. 3.5 we did not add noise to the spectra, therefore the fitted dust parameters do not depend on the value  $F_\nu^{\text{error}}$ .

The basic limitation of all the above described methods is the simple handling of the continuum and temperature of the radiating dust. Studies of protoplanetary disks have shown, that the silicate emission features arise from the uppermost optically thin disk layer (Chiang & Goldreich 1997; Mennschikov & Henning 1997) and the silicate emission zone can extend from less than 1 AU to a few tens of AUs in Herbig Ae systems (van Boekel et al. 2005a). Since the temperature in such wide range of radii should not be constant, it seems to be reasonable to apply a distribution of temperatures to model the  $10 \mu\text{m}$  silicate feature and the underlying continuum.

Here, we propose such a new method, which is more sophisticated compared to the above described models, but simple enough to be applied for large data sets. In this method we use a simple two-layer temperature distribution (hereafter TLTD method) in order to describe the temperature structure of the disk. In this TLTD approach the flux density at a specific frequency is given by

$$F_\nu = F_{\nu,\text{cont}} + \sum_{i=1}^N \sum_{j=1}^M C_{i,j} \kappa_{i,j} \int_{R_{\text{rim}}}^{R_{\text{out}}} \frac{2\pi r}{d^2} B_\nu(T_{\text{atm}}(r)) dr, \quad (7)$$

where

$$F_{\nu,\text{cont}} = C_0 \frac{\pi R_\star^2}{d^2} B_\nu(T_\star) + C_1 \int_{R_{\text{in}}}^{R_{\text{rim}}} \frac{2\pi r}{d^2} B_\nu(T_{\text{rim}}(r)) dr + C_2 \int_{R_{\text{rim}}}^{R_{\text{out}}} \frac{2\pi r}{d^2} B_\nu(T_{\text{mid}}(r)) dr. \quad (8)$$

Here  $R_{\text{in}}$  is the inner radius of the disk,  $R_{\text{rim}}$  is the outer radius of the puffed-up inner rim,  $R_{\text{out}}$  is the outer radius of the disk, while  $r$  is the distance to the central star and  $R_\star$  is the radius of the star.  $T_\star$  is the effective temperature of the central star, while  $T_{\text{rim}}(r)$ ,  $T_{\text{atm}}(r)$  and  $T_{\text{mid}}(r)$  are the temperature of the inner rim, disk atmosphere and the disk midplane, respectively. The mass fraction of a specific dust species is given by Eq. 3. The temperatures in the disk are given by

$$T_{\text{rim}}(r) = T_{\text{rim,max}} \left( \frac{r}{R_{\text{in}}} \right)^{q_{\text{rim}}} \quad (9)$$

$$T_{\text{atm}}(r) = T_{\text{atm,max}} \left( \frac{r}{R_{\text{Rim}}} \right)^{q_{\text{atm}}} \quad (10)$$

$$T_{\text{mid}}(r) = T_{\text{mid,max}} \left( \frac{r}{R_{\text{Rim}}} \right)^{q_{\text{mid}}} \quad (11)$$

In this fitting approach  $R_{\star}$ ,  $T_{\star}$  are given, while  $T_{\text{rim,max}}$ ,  $T_{\text{mid,max}}$ ,  $T_{\text{atm,max}}$ ,  $q_{\text{rim}}$ ,  $q_{\text{mid}}$ ,  $q_{\text{atm}}$ ,  $C_0$ ,  $C_1$ ,  $C_2$  and  $C_{i,j}$  have to be fitted. Apart from these parameters we also need to account for three radii ( $R_{\text{in}}$ ,  $R_{\text{rim}}$ , and  $R_{\text{out}}$ ).

Although there are three radii there are only two free parameters, namely their ratios  $R_{\text{out}}/R_{\text{rim}}$  and  $R_{\text{rim}}/R_{\text{in}}$ . The reason for that is the following. The replacement of boundaries in Eq. 7 and Eq. 8 from  $R_{\text{in}}$  to  $\alpha \cdot R_{\text{in}}$  and from  $R_{\text{out}}$  to  $\alpha \cdot R_{\text{out}}$  will not change the resulting dust composition. This behaviour is due to the  $C_i$  and  $C_{i,j}$  factors, which become  $\alpha^2 \cdot C_i$  and  $\alpha^2 \cdot C_{i,j}$  in the above described case. Since the mass fractions of different dust species is defined by Eq. 3,  $m_{i,j}$  does not depend on  $\alpha$ , although the total dust mass does. This means that, in a certain sense, the actual values of  $R_{\text{in}}$  and  $R_{\text{out}}$  are irrelevant, and the important parameter is rather the ratio between them. Since we do not apply radiative transfer calculations in the TLTD method, the radius and the temperature are not coupled to each other in a self consistent way and the role of the boundaries in Eq. 7 and Eq. 8 is only the weighting of different temperatures.

Thus, one can constrain  $R_{\text{out}}/R_{\text{rim}}$  and  $R_{\text{rim}}/R_{\text{in}}$  using the reasonable assumption that the outer radius of the disk is larger than the outer radius of the silicate emitting region. In this case, for each value of  $q_{\text{atm}}$  one can calculate the  $R_{\text{out}}/R_{\text{rim}}$  where the contribution of the outermost annulus to the total flux at  $10 \mu\text{m}$  equals to 0.1 % assuming a constant value for  $R_{\text{rim}}$  (the same holds for  $q_{\text{rim}}$  and  $R_{\text{rim}}/R_{\text{in}}$ ). One can then neglect the flux contribution of the annuli behind this radius.

This can be the most easily done by calculating the integrals in Eq. 7–8 over temperatures instead of radii. Thus, we can rewrite Eq. 7 in the form of

$$F_{\nu} = F_{\nu,\text{cont}} + \sum_{i=1}^N \sum_{j=1}^M D_{i,j} \kappa_{i,j} \int_{T_{\text{atm,max}}}^{T_{\text{atm,min}}} \frac{2\pi}{d^2} B_{\nu}(T) T^{\frac{2-q_{\text{atm}}}{q_{\text{atm}}}} dT, \quad (12)$$

where

$$D_{i,j} = \frac{q_{\text{atm}}}{T_{\text{atm,max}}^{-2/q_{\text{atm}}} R_{\text{in}}^2} C_{i,j} \quad (13)$$

The value of  $R_{\text{in}}$  is not important here, its role is only a dimensional matching, therefore, we can choose it arbitrarily, for instance to 1 AU. Eq. 8 can also be written in the same manner. The upper limits of the temperatures ( $T_{\text{rim,max}}$ ,  $T_{\text{atm,max}}$  and  $T_{\text{mid,max}}$ ) are fitted. Using the above described assumption, one can calculate the minimum temperature for each component

( $T_{\text{rim,min}}$ ,  $T_{\text{atm,min}}$  and  $T_{\text{mid,min}}$ ), where the contribution of the corresponding annulus to the total flux at  $10\ \mu\text{m}$  equals to 0.1%. The mass fraction of a given dust species is given by  $m_{i,j} = D_{i,j} / \sum_{i=1}^N \sum_{j=1}^M D_{i,j}$ . In order to compare the temperature distribution estimated by the TLTD method to the calculated distribution with the 2D RT code, we used Eq. 7 and Eq. 8 during the tests and the same  $R_{\text{in}}$  and  $R_{\text{out}}$  values were used in the fitting routine as in the 2D RT code.

The fitting of the temperatures at the boundaries ( $T_i$ ) and the power law indices ( $q_i$ ) is a highly non-linear problem which is not straightforward to solve. Beside the non-linear nature of the problem, the  $\chi^2$  surface can have numerous local minima, which makes the fit even more difficult. Most of the fitting routines like, e.g., *amoeba* (Press et al. 2001) are not able to find the global minimum or/and are very sensitive to the initial values. Therefore, we used the genetic optimization algorithm *pikaia* (Charbonneau 1995) in order to fit the temperatures and the power indices. It has been shown that this algorithm can efficiently find the global minimum even in a high dimensional parameter space with multiple local minima (Charbonneau 1995). This algorithm performs the maximization of a user defined function, thus we used the  $g(T, q) = 1/\chi^2$  function for that purpose. Once the temperature distribution is fixed, the evaluation of the  $C_{i,j}$  values is a linear problem. Thus, we used for that purpose the generalized linear least-square fitting routine of Lawson & Hanson (1974).

### 3. Results

In the following, we investigate the quality of the decomposition methods. We fitted our 2D RT model spectra between 7 and  $14\ \mu\text{m}$  since this is a widely used wavelength range for spectral decomposition in the case of *Spitzer* observations. In order to measure the quality of the fits we calculated the mass-averaged grain size of the amorphous material and the crystallinity fraction from the chemical composition estimated by the fitting methods. We use these parameters, since grain growth and crystallisation are among the key processes occurring during the evolution of protoplanetary dust. The evolutionary status of dust grains is, therefore, usually characterized by these two parameters which are commonly derived from the observations. For a more straightforward analysis of the results, we defined a normalized crystallinity as the fraction of silicate mass in crystals. The total crystallinity is the fraction of total dust mass in crystalline silicates. The advantage of the normalized crystallinity is that, for a given, fixed dust composition, its value does not change if we exclude carbon from the fitting procedure.

### 3.1. Disk structure and stellar type

In the following, we investigate the effect of the disk structure and the stellar type on the fitted dust composition. There are three questions we address in this section. (i) How large is the *average* deviation of the dust parameters fitted by a specific method from the input parameters? (ii) How large is the scatter around the mean dust parameters? (iii) Is there any correlation, within the scatter, between the dust composition and the flaring index, the inclination angle or the stellar type? In order to quantify the answers for these questions we compute the mean value, the standard deviation around the mean and the Pearson's correlation coefficient between the chosen parameters and flaring index, inclination angle and the stellar temperature. The Pearson's correlation coefficient ( $r$ ), which is frequently used to measure the linear dependence of two variables ( $x, y$ ), is calculated as

$$r = \frac{n \sum x_i y_i - \sum x_i \sum y_i}{\sqrt{n \sum x_i^2 - (\sum x_i)^2} \sqrt{n \sum y_i^2 - (\sum y_i)^2}}, \quad (14)$$

where  $n$  is the number of data points. In order to investigate the significance of the Pearson's correlation coefficient, one can calculate the probability that the observed relation can be produced by random distribution with the same sample size ( $n$ )

$$p(r, n) = \frac{2\Gamma\left(\frac{n-1}{2}\right)}{\sqrt{\pi}\Gamma\left(\frac{n-2}{2}\right)} \int_{|r|}^1 (1-u^2)^{(n-4)/2} du \quad (15)$$

(see, e.g., Taylor 1997)

The normalized crystallinity values obtained by the COS method show a large scatter, overestimating and (in a few cases, e.g., for Brown Dwarf in CS series) underestimating the real value (see Fig. 2 *Left*). On average, the normalized crystallinity is overestimated by a factor of  $2.8 \pm 1.9$  and it correlates with the stellar temperature ( $r=0.53$ ,  $p=10^{-6}$ ) and with the flaring index ( $r=0.47$ ,  $p=5 \cdot 10^{-5}$ ). The ST method overestimates the normalized crystallinity (by a factor of  $4 \pm 1.1$ ), which does not depend on the stellar temperature, but it correlates directly with the flaring index ( $r=0.63$ ,  $p=3 \cdot 10^{-9}$ ). There is also a hint of a weak inverse correlation between the crystallinity and the inclination angle ( $r=-0.3$ ,  $p=0.01$ ). The TT method overestimates the normalized crystallinity by a factor of  $1.8 \pm 0.25$ , which depends weakly on the stellar temperature ( $r=-0.34$ ,  $p=0.003$ ) but is independent of the flaring index or of the inclination angle.

The total and normalized crystallinity fraction estimated by the TLTD method is the closest to the input value in general. This method overestimates the crystallinity by a factor of  $1.2 \pm 0.13$ . The crystallinity does not depend on the stellar type but it depends weakly on the flaring index ( $r=-0.47$ ,  $p=2 \cdot 10^{-5}$ ). The effect of the inclination on the fitted dust

composition is the weakest for the TLTD method. Within the studied range of inclination angles ( $0^\circ$ – $70^\circ$ ) the scattering in the crystallinity due to the inclination angle is less than 1% for the TLTD method. It can also be seen in Fig. 2 *Left* that the inclination has the smallest effect on the results of the TLTD method, indicated by the error bars, compared to other methods.

Although, the input dust composition to the 2D RT disk models did not contain large ( $6\mu\text{m}$ ) enstatite grains at all, the bulk of the crystalline silicates, predicted by the TT method ( $\sim 60\%$  in terms of the total crystal mass), is in the form of large enstatite grains. The TLTD method also suffers from the overestimation of the large enstatite fraction, while the ST method has this problem just in a few cases. The overestimation of large enstatite content is probably not related to the type of the decomposition method, since all the methods have this problem, but it is probably related to the similarity between the optical data of large enstatite and other dust species. The mass absorption coefficients of the large enstatite grains can be reproduced, in the fitted wavelength range, by a linear combination of small olivine, small carbon and medium sized enstatite grains. If this problem is really caused by the degeneracy of the optical data, we should get better results if we use a broader wavelength interval for the fits. The probability, that two dust species have similar optical data, is lower for a broader wavelength range. We will discuss the effect of the fitting range in more detail in Sec. 3.3.

The mass-averaged grain size of the amorphous silicates has also been calculated from the fit results (Fig. 2 *Left*). Since this quantity can change by more than an order of magnitude ( $0.1$ – $6.0\mu\text{m}$ ) we used the standard deviation of the logarithm of grain size instead of the grain size itself to quantify the average and scatter of this parameter. The COS method overestimates this quantity in all cases by a factor of  $2.6^{+2.0}_{-1.1}$ . This fitting approach predicts larger grains for lower stellar temperatures ( $r=-0.53$ ,  $p=5 \cdot 10^{-5}$ ) and for flatter disks ( $r=-0.46$ ,  $p=5 \cdot 10^{-5}$ ), but the results do not depend on the studied range of inclination angles ( $0^\circ < i < 70^\circ$ ). The ST method underestimates the mass-averaged grain size by a factor of  $0.42^{+0.7}_{-0.3}$ . The results of the ST method depend only on the stellar temperature, predicting larger grains for lower stellar temperatures ( $r=-0.51$ ,  $p=4 \cdot 10^{-6}$ ). The TT method also underestimates the average grain size for T Tauri and Brown Dwarf disk models, while the fitted grain size is larger than the input value for Herbig Ae spectra. On average the TT method underestimates the average grain size by a factor of  $0.7^{+1.9}_{-0.5}$ , showing a larger scatter around the mean value and correlating weakly with the stellar temperature ( $r=0.51$ ,  $p=4 \cdot 10^{-5}$ ). The TLTD method overestimates the mass-average grain size of the amorphous material by a factor of  $1.8^{+0.4}_{-0.4}$  and the grain size also correlates with the flaring index ( $r=-0.6$ ,  $p=10^{-8}$ ). It is interesting to note, that this correlation decreases towards lower stellar temperatures ( $r=-0.7$ ,  $r=-0.6$  and  $r=-0.3$  for Herbig Ae, T Tauri and Brown Dwarf models,

respectively).

### 3.2. Featureless grains

The amount of "featureless" grains (like, e.g., carbon) can also be important in evaluating the fraction of crystalline grains and mass-averaged grain size. Due to their smooth, featureless opacity curve in the fitted region (7–14  $\mu\text{m}$ ), the optically thin emission of such grains acts like a continuum. Thus, there is a degeneracy between the optically thin emission of featureless grains and the optically thick emission of different parts of the disk. This degeneracy can have a strong effect on the results of the fits. The importance of this degeneracy is well reflected by the fact, that the ST method estimated a very high fraction of amorphous carbon (up to 90% in terms of total dust mass) in all test cases. The TT method also had this problem in several cases, while the TLTD method did not show such a behavior. We discuss this behaviour in more detail in Sec. 4.

In order to study the role of carbon grains in our fits, we tried to fit the same model spectra *without* carbon (see Fig. 3), however carbon is present in the input dust composition<sup>1</sup>. We want to note, that real observations were always fitted without carbon if the COS, the ST or the TT method has been used for spectral decomposition. In the case of the COS method the resulting crystallinity is completely underestimated compared to the input value (down to 0% for Brown Dwarf spectra, see Fig. 3 *Left*). Moreover, the COS method fits lower crystallinities for lower stellar luminosities ( $r=0.75$ ,  $p=10^{-14}$ ). The resulting crystallinity fraction of the ST is overestimated by a factor of  $4\pm 1$  compared to the 'real' value. The resulting crystallinity in this case depends weakly on the stellar temperature ( $r=-0.4$ ,  $p=6 \cdot 10^{-4}$ ) and on the flaring index ( $r=-0.43$ ,  $p=1.5 \cdot 10^{-4}$ ) and the fitted crystallinity is higher compared to the fits with carbon. The TT method underestimates the crystallinity slightly (by a factor of  $0.85\pm 0.2$ ). The results are sensitive to the inclination of the disk, indicated by the larger error bars in Fig. 3 *Left*. The results do not correlate with the flaring index, or stellar temperature but depend weakly on the inclination angle ( $r=0.43$ ,  $p=1.5 \cdot 10^{-4}$ ). The average crystallinity evaluated by the TLTD method is overestimated by a factor of  $1.5\pm 0.4$  on average. The normalized crystallinity fitted by the TLTD method is less sensitive to the inclusion or exclusion of featureless grains compared to other methods.

The mass-averaged grain size of the amorphous silicates is presented in Fig. 3 *Right* for fits without carbon among the fitted dust species. The exclusion of the featureless dust species results in higher average grain sizes for the silicate species for the COS and TT

---

<sup>1</sup>In reality carbon grains can very well be an important grain component of protoplanetary disks.

methods by a factor of 2 and 1.4, respectively, compared to the fits with carbon. There is a strong inverse correlation between the average grain size, predicted by the TT method, and the stellar temperature ( $r=-0.42$ ,  $p=2 \cdot 10^{-4}$ ) and the flaring index ( $r=-0.66$ ,  $p=2 \cdot 10^{-10}$ ). In the case of the ST method the resulting mass-averaged grain size of the amorphous silicates decreases slightly (by 20%) compared to the fits with carbon. The average grain size estimated by the TLTD method decreases on average compared to fits with carbon by 20%. Furthermore, the predicted grain size correlates with the flaring index ( $r=-0.49$ ,  $p=8 \cdot 10^{-6}$ ).

### 3.3. Wavelength range

The wavelength range, for ground-based observations, is usually limited to 8–13  $\mu\text{m}$  due to the strong absorption of the Earth’s atmosphere both shortward and longward of this range. For *Spitzer* data, the broadest possible wavelength range is determined by the instrumental capabilities of the IRS instrument (5.2–38  $\mu\text{m}$ ). It may be important how the wavelength range for the fit is chosen. A narrower wavelength range corresponds to a narrower range of temperatures one has to take into account in the modelling of the feature<sup>2</sup>. On the other hand, a narrower wavelength range can result in a higher degeneracy among the optical data of different dust species. This effect results in a higher uncertainty in the derived dust parameters. In order to investigate how the results depend on the choice of the selected wavelength range, we fitted all the T Tauri spectra with different wavelength domains. Three wavelength regions were used for the ST and TT methods (8–13  $\mu\text{m}$ , 7–14  $\mu\text{m}$ , 7–17  $\mu\text{m}$ ), while these ranges were supplemented by a fourth very broad range for the TLTD method (5–35  $\mu\text{m}$ ).

The results showed that, for the COS, ST and TT method, the 7–14  $\mu\text{m}$  range gives the best results in general. However, the estimated large enstatite particle fraction is much closer to the ”real” values, using a broader wavelength range (see Fig. 4*Right*). The estimated mass-averaged grain size of the amorphous silicates is underestimated with the other wavelength intervals (roughly by a factor of two) compared to the results of the fit using the 7–14  $\mu\text{m}$  domain (see Fig. 4*Right*). In the case of the TLTD method, the broader wavelength range results in better estimates of all parameters. It is interesting to note that we get the best results using the 7–17  $\mu\text{m}$  range and the results become worse if we use the broadest range between 5 and 35  $\mu\text{m}$ . Using the 7–17  $\mu\text{m}$  wavelength interval the mass-average grain size

---

<sup>2</sup>For a narrower temperature range, the assumption of a fixed dust composition is certainly better justified compared to a wide range in temperatures which corresponds to a larger disk region.

and total crystallinity, fitted by the TLTD method, are overestimated by a factor of 1.45 and 1.05, respectively. In this case, the only correlation we found is the dependence of the mass-averaged grain size on the flaring index of the disk ( $r=-0.7$ ,  $p=8 \cdot 10^{-12}$ ) Using the broadest wavelength range, the average grain size is underestimated by 70 %, while the total crystallinity is overestimated by a factor of 1.75. One reason for that can be that even the TLTD method is too simple to describe the temperature structure of a real disk correctly. Another reason for the worse results can be found in the optical data of the different silicate species. While the crystalline silicates have sharp features in the 20–30  $\mu\text{m}$  region, the optical data of large amorphous silicate grains are very smooth, which makes it difficult to recognize this component.

The normalized crystallinity as a function of mass-averaged grain size is presented in Fig. 5 for the best configuration of each method. The results of the TT method seem to be relatively close to that of the TLTD method. However, the fitted dust composition obtained by the TT method suffers from the overestimation of the abundance of large enstatite grains. The predicted amount of large enstatite grains was closer to the input value using a broader wavelength range (7–17  $\mu\text{m}$ ) regardless of the spectral decomposition method. This fact proved our former assumption that the overestimation of the large enstatite grains is the result of the degeneracy between the optical data of the large enstatite grains and other dust species in the narrower wavelength interval.

### 3.4. Large grains

It is well known, that the strength of the spectral features in the 10  $\mu\text{m}$  region decreases with increasing grain size (see, Fig. 1). Therefore the emission of dust grains larger than 2  $\mu\text{m}$  are usually neglected during the spectral decomposition. Although the strength of the 10  $\mu\text{m}$  feature of the amorphous silicates is much weaker for a grain size of 6  $\mu\text{m}$  than for 0.1  $\mu\text{m}$  the feature strength is not completely zero. In this study, we included also 6.0  $\mu\text{m}$  sized grains in the input dust composition to the 2D RT code. Dust grains with such size are probably present in the disk atmosphere if grain growth occurs in the disk, although their abundances depend on the turbulence and sedimentation processes. In order to test the importance of the largest grain population (in case of ground-based observations), all T Tauri spectra were fitted using a wavelength range of 8–13  $\mu\text{m}$  and excluding all 6  $\mu\text{m}$  sized grains from the fit, although large grains were present in the 2D RT disk models. In this case we were interested how well the properties of the smallest grain populations can be recovered by the methods. Therefore, during the comparison of the fitted dust mixtures with the input composition we used only the 0.1  $\mu\text{m}$  and 1.5  $\mu\text{m}$  sized grains, which is the



usual approach in the literature.

The results are summarized in Fig. 6. It can be easily seen that the dust parameters fitted by *all* methods deviates from the input dust parameters. If we included large grains in the fit, their estimated fraction by the ST method was less than a few percent, therefore their effect on the fit is obviously weak. The resulting dust parameters of the TT method, get further away from the right values if we excluded the large grains from the fit. The smaller mass-averaged grain size is caused by the excluded large amorphous grains, the fraction of which is significant if we included them in the fit. The smaller estimated crystallinity is a result of the exclusion of large enstatite grains. The results of the TLTD method were almost identical to the input dust mixture giving far the best results among the tested methods. The differences between the resulting dust composition including/excluding large grains in/from the fit can be related to the disk structure and will be discussed in detail in Sec. 4.3.

### 3.5. The influence of simulated noise

Observations always suffer from uncertainty in the observed quantities and these errors naturally affect the parameters derived from the observational data. Since one cannot avoid the effect of noise, it is important to know how sensitive the applied method is to the noise level and how the uncertainty of the derived parameters can be estimated from the observational errors. In the case of the spectral decomposition of the silicate feature around  $10\ \mu\text{m}$ , it is very difficult to describe the error propagation by analytical formulas. A simpler way to estimate the uncertainty in the fitted chemical composition is a Monte Carlo type of error estimation (e.g., van Boekel et al. 2005b). In this kind of error estimation, a normally distributed noise is added to the spectrum, scaling the width of the distribution to the simulated observational uncertainty in the flux value. Then the resulting spectrum should be fitted. This procedure should be repeated many times. Then the standard deviation of the resulting mass fractions will be the uncertainty of the derived dust compositions.

We used the spectrum of a T Tauri star with a moderately flared disk and an inclination of  $45^\circ$  for testing the effect of different noise levels on the results of the TLTD method. We studied the effect of noise on ground- and space-based observations, using a wavelength range of  $8\text{--}13\ \mu\text{m}$  and  $7\text{--}17\ \mu\text{m}$ , respectively. Three different noise levels have been used in these tests with an  $F_\nu^{\text{error}}/F_\nu^{\text{observed}}$  of 0.1, 0.01 and 0.001, corresponding to a signal-to-noise (S/N) ratio of 10, 100 and 1000, respectively. We want to note, that the noise level was assumed to be independent of wavelength, which can be good approximation for bright sources, while this assumption is certainly not correct for faint sources with strong silicate feature. After 100 spectra have been generated and fitted for each noise level, we studied the average chemical

composition over the 100 spectra, the mass-averaged grain size and normalized crystallinity and the scattering around the average values. The latter two parameters have the advantage that, even for low S/N, they can be more certainly evaluated than the mass fraction of a single dust component.

The normalized crystallinity as a function of mass-averaged grain size, derived by the TLTD method, is presented in Fig. 7 for simulated ground-based observations (8–13  $\mu\text{m}$ ). It is easy to see, that the uncertainty in the value of crystallinity and mass-averaged grain size (obviously) increases with increasing noise level. Moreover, for lower signal-to-noise ratio the average value of the crystallinity and the average grain size increases. For a S/N of 100 the average value of the crystallinity and the mass-averaged grain size are overestimated by a factor of 1.5 and 3, respectively, compared to the input values. The scattering of the individual points is not perfectly symmetric to the mean value. The uncertainty of the value of the crystallinity is higher above the mean value than below that. The uncertainty on the value of crystallinity for a S/N of 100 is +11% -7% in an *absolute* sense (i.e. in terms of the total silicate mass). In the case of the average grain size the uncertainty on the average value is +1  $\mu\text{m}$  and -1.5  $\mu\text{m}$ .

For space-based observations (see Fig. 8, 7–17  $\mu\text{m}$  range), the scattering of the normalized crystallinity and mass-averaged grain size decreases compared to that of the ground-based observations. Furthermore the average values of these quantities are closer to the input value of the 2D RT codes using the broader wavelength range. For a S/N of 100 the average value of the crystallinity and the mass-averaged grain size are higher than the input value by a factor of 1.26 and 1.44, respectively. The uncertainties on the average value of the crystallinity is 5% in an *absolute* sense (i.e. in terms of the total silicate mass). In the case of the average grain size the uncertainty on the average value is 0.8  $\mu\text{m}$ .

Although the signal-to-noise ratio of the data is of fundamental importance, the uncertainty of the fitted dust parameters, caused by the noise, depends on the actual dust composition and the optical constants. Since the crystalline silicates have usually strong, narrow and sharp features their abundances can be constrained better, even for low signal-to-noise ratio, than the abundances of the amorphous silicates with broad, flat features. Therefore, it is obvious, that the higher the crystallinity the easier it is to determine its value.

## 4. Discussion

Our results clearly indicate that the evaluation of the chemical composition of dust in protoplanetary disks from mid-infrared spectra is not straightforward even if do not have to consider the uncertainties in the optical constants of the dust grains. The resulting dust parameters strongly depend on the assumed continuum below the feature and the assumed temperature(s) of dust grains emitting at the considered wavelengths. In the following, we will discuss the reasons why the results of different methods deviate from the input dust composition, and which effects should be taken into account during the analysis of mid-infrared dust features.

### 4.1. Temperatures in the feature

Both the ST and TT methods assume that *the source function underlying the emission in the 10  $\mu\text{m}$  feature can be well approximated by a blackbody curve with a single effective temperature.* van Boekel et al. (2005a) have shown that the region where the 10  $\mu\text{m}$  emission comes from can extend from less than 1 AU to several tens of AU in Herbig Ae systems. They also have shown that the mid-infrared radiation, emitted by the different annuli (with different temperatures), contributes to the total observed flux in this wavelength regime significantly. We also investigated the temperature structure of the 2D RT disk models in the region where the bulk of the 10  $\mu\text{m}$  emission originates. Images of the disk models were calculated at 10  $\mu\text{m}$  and then the cumulative flux as a function of radius was used to determine the size of the region from which 70% of the total flux originates (Fig. 9a). In order to characterize the temperature in the disk atmosphere we evaluated the temperature along the line where the radial optical depth  $\tau_{0.55\mu\text{m}}$  reaches unity in the disk, using the definition of Chiang & Goldreich (1997). From Fig. 9b it can be seen, that the temperature in the disk atmosphere changes significantly in the region where the silicate emission comes from. On the other hand the changes of the surface density of the disk atmosphere as a function of radius are just marginal and they depend on the flaring index. Since the silicate emission feature is produced by a convolution of optical depth (or surface density) and the Planck function at different temperatures, it now becomes obvious why the simple "isothermal" models give poor results. A sum of different Planck curves with these rather different temperatures cannot be reproduced by a single Planck curve.

Since we used the same  $R_{in}$  and  $R_{out}$  both in the 2D RT code and in the TLTD fitting method, we can compare the fitted temperature distribution with the temperature structure of the 2D RT models. Fig. 9b shows that the TLTD method can efficiently evaluate the temperature distribution in the disk atmosphere. The ratio of the slope of the fitted atmosphere

temperature by the TLTD method and that of the 2D RT code was  $0.88 \pm 0.07$  averaging over all the fitted spectra. The same ratio for the boundary temperature ( $T_{\text{atm,max}}$ ) was  $1.3 \pm 0.6$ .

## 4.2. Temperatures in the optically thick continuum

Another assumption of the ST and TT methods is that *the continuum below the emission feature can be described by a Planck function with a single temperature*. Using the passive irradiated disk model of Dullemond et al. (2001), the continuum emission in that region has four components: emission of the central star, the puffed-up inner rim, the disk midplane and the emission of the featureless (e.g., carbon) grains in the disk atmosphere. In general, shortward of  $\sim 8 \mu\text{m}$ , the continuum is dominated by the emission of the hot inner rim of the disk with decreasing flux towards longer wavelengths. At wavelengths longer than  $12\text{--}14 \mu\text{m}$  most of the continuum emission comes from the disk midplane with increasing flux towards longer wavelengths. Thus, the slope of the continuum should change in the  $8\text{--}12 \mu\text{m}$  region in order to match the decreasing flux of the inner rim and the rising flux of the midplane. The turn-over point, where the slope changes is determined by the balance of the rim and midplane components (which is set by the disk geometry and the inclination) and by the featureless grain (e.g., carbon) content of the dust. One of the reasons for the poor performance of the COS, ST and TT methods lies in their incapability to fit a continuum with such a shape.

The ST method simply cannot reproduce the real continuum, since the temperature in the continuum and in the feature is the same in this approach (see Fig. 10a). The only way to fit the real continuum is the inclusion of large amorphous carbon, the mass absorption coefficient of which increases with wavelength in this region. Therefore, this method fitted an unrealistic amount of carbon ( $\sim 70\text{--}90\%$  of the total mass) in order to fit the real continuum.

In the case of the TT approach two distinct solutions exist for the fit, which can be easily seen in Fig. 11 as the  $\chi^2$  space has two minima. This kind of  $\chi^2$  space is characteristic for the TT method during the fitting of the spectrum of a Class II source, using the classification scheme of Lada & Wilking (1984) and related to the fit of the continuum. One of the two minima has a high continuum temperature ( $\sim 600$  K) and low feature temperature ( $\sim 200$  K, see Fig. 10a). In this case, the resulting dust composition overestimates the mass fraction of large ( $a = 6 \mu\text{m}$ ) carbon grains. In this solution the real continuum is fitted with the high temperature continuum component shortward of  $\sim 10 \mu\text{m}$ , while at longer wavelengths the real continuum is fitted by the optically thin emission of carbon grains. In the case of the other minimum, the feature has a higher temperature than the continuum and the resulting amount of carbon is very well estimated. On the other hand the silicate grains, producing the

$10\ \mu\text{m}$  feature, are significantly larger compared to those in the other solution. The reason for the larger average grain size is that the mass absorption coefficient of the large ( $6\ \mu\text{m}$ ) amorphous grains is higher than that of the smaller ones shortward of  $\sim 8.5\ \mu\text{m}$ . Therefore the real continuum emission at longer wavelength is fitted with the single temperature continuum of the TT method, but shortward of  $8.5\ \mu\text{m}$  the real continuum is fitted by including large amorphous grains.

The subtraction of the continuum can be a better solution if, and only if, the real continuum is known, otherwise the subtraction of the continuum introduces an additional uncertainty in the results. The highest uncertainty in the COS method is that it tries to extrapolate the continuum by fitting a few data points. Therefore, the fitted continuum is very sensitive to the wavelength ranges in which it has been fitted. Although, the COS method estimated the mass-averaged grain size in a few cases equally well as the TLTD method, the total crystallinity was deviating most strongly from the real value.

We compared the temperature profile of the disk midplane calculated by the 2D RT code to the fitted temperature distribution by the TLTD method (Fig. 9c). In this case the temperature distribution in the 2D RT model was calculated along the line where the vertical optical depth in the disk at  $10\ \mu\text{m}$  equals unity. One can see that the TLTD method overestimated the temperature compared to that of the 2D RT code. Furthermore the slope of the temperature distribution is very low. The ratio between the fitted power-law indices and the calculated one by the 2D RT code was  $0.33 \pm 0.33$ , and that of the boundary temperature was  $1.4 \pm 1.0$ . The reason for the difference between the fitted and the 'real' midplane temperature in general is caused by the fact that even the TLTD method is too simple to represent the temperature structure of a protoplanetary disk. In contrast to the  $7\text{--}8\ \mu\text{m}$  region, longward of  $12\ \mu\text{m}$  the continuum cannot be unambiguously determined, since the dominant contributor to the total emission is still the disk atmosphere. Moreover, there is a degeneracy between the optically thin emission of the featureless grains and the optically thick disk emission. In a 2D RT code the layer where the 'midplane' emission originates depends strongly on the disk geometry, inclination angle, and of course on the wavelength. During the comparison of the results of the TLTD method and the 2D RT code we made the simplifying assumption that the layer, where the 'midplane' emission comes from, is where the vertical optical depth at  $10\ \mu\text{m}$  equals unity, which is only true for face-on orientation.

### 4.3. Explanation of the correlations

The shape and strength of the silicate feature around  $10\ \mu\text{m}$  is affected by the disk structure, the inclination and the stellar type in a complex way. The efficiency of a spectral

decomposition method depends on how it can handle these effects. In the former two sections we discussed why the single and two temperature approximations or a continuum subtraction are insufficient to model the temperature structure of the silicate emission zone in a protoplanetary disk. This weakness of the fitting routines can lead to a large scatter in the derived dust parameters. Here, we discuss how and why the derived dust parameters can depend on the geometry of the source or the stellar type. If such an "artificial" dependence is not properly understood, the comparison of grain parameters derived for different source types can be misleading.

The effect of the stellar temperature on the mid-infrared silicate features can be much stronger than it is usually thought. Under the assumption of an identical star-to-disk luminosity ratio and disk structure, the contribution of a Brown Dwarf ( $T_{\text{eff}}=2500$  K) to the  $10\ \mu\text{m}$  emission is roughly 44 times higher than that of a Herbig Ae star ( $T_{\text{eff}}=9500$  K). In Fig. 12a it can be seen that this increasing "stellar" contribution toward lower effective temperatures results in lower peak over continuum ratios of the  $10\ \mu\text{m}$  feature *without* changing the parameters of the dust model. This phenomenon naturally explains the strong inverse correlation between stellar temperature and the temperature fitted by the ST method ( $r=-0.84$ ) and the continuum temperature fitted by the TT method ( $r=-0.92$ ). Moreover, the feature temperature over continuum temperature ratio predicted by the TT method directly correlates with the stellar temperature ( $r=0.93$ ). The continuum temperature is always higher than the feature temperature for Brown Dwarfs and mostly for T Tauri stars. This kind of solution seems to be unphysical (compared with the radiative transfer solution of the problem (Chiang & Goldreich 1997; Menshchikov & Henning 1997)). The TT method is not a solution of the radiative transfer problem and simply fits the dominant continuum component. As the stellar contribution becomes the dominant continuum component for lower stellar temperatures, the TT method fits higher continuum temperatures. This behaviour of the TT method leads to a strong "artificial" inverse correlation between the stellar temperature and the mass-averaged grain size of the amorphous silicates if we fit the spectra without carbon. The TLTD method is much less affected by this effect, since the stellar contribution is already included in the fit. The average grain size does not depend on the stellar temperature if we include carbon in the fit, but it does if we exclude carbon, although this correlation is weaker compared to that of the other methods ( $r=-0.67$ ).

The effect of the flaring index, i.e. the disk geometry, is more complex than that of the stellar temperature. As Kessler-Silacci et al. (2007) have shown the radius of the zone where the  $10\ \mu\text{m}$  emission comes from can decrease for flattened disks compared to flared disks. Thus the decrease of the flaring index can have two important consequences concerning the  $10\ \mu\text{m}$  silicate emission band. One effect is that the contribution of the midplane component to the total flux below the silicate feature decreases toward flattened

disks (Dullemond & Dominik 2004). In other words, the dominant continuum temperature shifts toward higher values toward lower flaring indices. Moreover, the amount of optically thin matter decreases more rapidly with radius in flattened disks than in flared disks (Kessler-Silacci et al. 2007). This behaviour leads to the decrease of the height of silicate emission feature above the continuum toward flattened disks (see Fig. 12*b*). The  $10\ \mu\text{m}$  feature is, however, less affected by the disk geometry for Brown Dwarfs compared to Herbig stars, since the relative contribution of the "stellar" component to the continuum emission at  $10\ \mu\text{m}$  becomes stronger for lower stellar temperatures. This behaviour explains why the temperature fitted by the ST method inversely correlates with the flaring index for Herbig Ae spectra ( $r=-0.85$ ) but not for Brown Dwarf spectra ( $r=-0.33$ ). The continuum temperature as well as the continuum over feature temperature ratio predicted by the TT method behaves exactly the same. This is likely the reason why the mass-averaged grain size inversely correlates with the stellar temperature for all the methods (however the strength of the correlation depends on the method), but this correlation is the strongest for Herbig Ae spectra and almost disappears for Brown Dwarf spectra. The TT method is an exception as the predicted grain size correlates inversely with the flaring index also for Brown Dwarf spectra.

The results of none of the methods show a close correlation with the inclination angle. The scatter in the derived dust parameters is the smallest for the TLTD method (more than a factor of two compared to other methods). It can be seen in Fig. 12*c*) that the changes in the inclination angle modifies the relative contribution of different (mainly continuum) components (i.e., star, inner rim, and disk midplane) to the total flux. The high temperature continuum components (the star and the inner rim) becomes stronger for higher inclination angles (close to edge-on) while at the same time the midplane component becomes weaker. The TLTD method can better handle this behaviour due to the  $C_0$ ,  $C_1$ ,  $C_2$  factors. We want to note, that the TLTD method, in this form, cannot handle edge-on disks where the silicate emission band is affected by the extinction of the outer parts of the disk.

In general, all these findings should serve as a warning, that correlations between grain parameters and disk/stellar properties can be artificially produced by limitations of the spectral decomposition methods.

#### 4.4. Degeneracies in the optical data

Another problem in the spectral decomposition of the mid-infrared silicate feature can be the degeneracy among the optical data of the fitted dust species. If the mass absorption coefficients of two dust species are very similar to each other it will be hard to identify

them separately in the observed spectrum regardless of the applied spectral decomposition method<sup>3</sup>.

Similar to van Boekel et al. (2005b), we also investigated this effect by fitting the mass absorption coefficients of each dust species with that of the other species. In order to quantify the quality of the fit we calculated the average deviation of the best fit model from the mass absorption coefficient of the analyzed dust species ( $\langle \sigma_\nu \rangle$ ), where

$$\sigma_\nu = \left( \frac{(\kappa_\nu^{\text{model}} - \kappa_\nu)^2}{(\kappa_\nu)^2} \right)^{1/2}. \quad (16)$$

Here,  $\kappa_\nu$  is the mass absorption coefficient of the dust species under consideration, and  $\kappa_\nu^{\text{model}}$  is the mass absorption coefficient of the best fit model. The  $\sigma_\nu$  value for each fit is presented in Fig. 13.

It can be seen, that for a wavelength range of 8–13  $\mu\text{m}$  the optical data of pyroxene-type amorphous silicates and large (6  $\mu\text{m}$ ) enstatite can be well reproduced by the other dust species. For this wavelength range there are several dust species for which the  $\langle \sigma \rangle$  value is less than 0.1, implying that they can be on average reproduced at a 10 % level by a linear combination of other dust species. If one has a signal-to-noise ratio of 10 these dust species cannot be identified in the spectrum due to the similarities of the mass absorption coefficients. It can be seen from Fig. 13 *b* and Fig. 13 *c* that  $\langle \sigma \rangle$  increases with the width of the wavelength range used for the fit. On the other hand, the comparison of Fig. 13 *c* and Fig. 13 *d* shows that, for a wavelength range of 5–35  $\mu\text{m}$ , the optical data of a specific dust species can be equally well reproduced by the other species, as for a wavelength range of 7–17  $\mu\text{m}$ . If the mass absorption coefficients of two dust species are very similar to each other, then they cannot be identified in the spectrum separately *independently from the applied spectral decomposition method*. We recommend to perform this kind of analysis for any new dust model, in order to recognize and understand the possible degeneracies.

During this analysis we did not take into account the continuum since the shape of the fitted continuum depends on the applied spectral decomposition method and we were interested in the degeneracies among the mass absorption coefficients only. The applied continuum has probably the strongest effect on the featureless dust component (in our case on the carbon). Although the real continuum (the shape of which is the best reproduced by the TLTD method) is not a straight line as the mass absorption coefficient of the 6  $\mu\text{m}$

---

<sup>3</sup>Dust components will not behave the same in very wide wavelength regions. Radiative transfer calculations would then require to obtain dust temperatures which would allow to distinguish between the components.



sized amorphous carbon grains in the fitted domain, it can still be very difficult to identify such featureless dust species, especially using a narrow wavelength range (8–13  $\mu\text{m}$ ). The mass absorption coefficient curve of the 0.1 and 1.5  $\mu\text{m}$  sized amorphous carbon grains can also be hardly separated from the combination of inner rim and disk midplane emission. Therefore, one should be careful during the interpretation of the carbon fraction fitted by simple methods like those ones tested in this paper.

In order to test the significance of the detection of a given dust component an F-test can be used (e.g. Min et al. 2007). Synthetic observations should be created by adding simulated noise to the observed spectrum as it has been done in Sec 3.5. These synthetic spectra should be fitted with and without the dust component under consideration. The ratio of the two  $\chi^2$  distribution (with and without the dust component) gives the F-distribution. After the mean value and the standard deviation ( $\sigma$ ) of the F-distribution has been calculated one can determine the distance of the mean (in terms of  $\sigma$ ) from unity, which gives the significance level for the detection of the dust component. If a component, which is significantly present in the spectrum, is added to the fit the  $\chi^2$  should decrease, while for an insignificant detection the  $\chi^2$  does not change. One should, however, be careful with the F-test during the significance test, since the F-test assumes that all components are independent from each other, i.e. there is no degeneracy among the components. Without any knowledge on the degeneracies among the dust components one should perform an F-test not only for each dust species but also for all possible linear combination of them in order to draw the right conclusion from the test. Another possibility can be that before the F-test is done one performs the above described simple analysis of the mass absorption coefficients (fitting the mass absorption coefficient of a given dust species with a linear combination of others). Such an analysis gives an indication for which dust species an F-test should be done carefully.

The general performance of a spectral decomposition method is determined by two important effects, which must be handled together and which act in opposite directions. One problem is the degeneracy/similarities of the optical data of the fitted dust species, which requires the broadest possible wavelength range. The other effect is linked to the fitted temperature(s). All the simplifying assumptions of the above described simple methods, as for instance the assumption of an average temperature, becomes more valid for a narrower wavelength interval (i.e., a narrower range of temperatures), compared to a broad one. The optimal wavelength range for a specific method is therefore determined by the balance of these two effects. Due to the assumption of a single temperature, all previously used methods can handle just a limited wavelength range (8–13  $\mu\text{m}$  or 7–14  $\mu\text{m}$ ), where the similarities of the optical data can play an important role for low S/N data. An advantage of the TLTD method over the other methods is, that one can extend the fitted wavelength interval by applying a temperature distribution. On the other hand, the TLTD method is still an

*approximate* method, which means that one cannot apply this method to an arbitrary broad wavelength range. An optimal wavelength range can be the interval between 7 and 17  $\mu\text{m}$ . For this interval, the differences between the optical data of the fitted dust species are roughly as high as for a wavelength range of 5–35  $\mu\text{m}$ , applying our dust model. Moreover, the 7–17  $\mu\text{m}$  range is narrow enough to apply our approximate temperature determination and allows to make the assumption that the grain composition does not change dramatically with radius.

#### 4.5. Limitations of the TLTD method

Although the new TLTD method returned dust parameters closest to the input dust mixture in most cases, this method has its limitations as well as any other method based on simplifying assumptions. During the derivation of Eq. 12 we assumed that the optical depth in the disk atmosphere does not depend on the radial distance. In a real disk the optical thickness in the disk atmosphere depends on the radius. However this dependence is marginal and depends on the flaring index. Therefore, the assumption of constant optical thickness in the disk atmosphere as a function of radius seems to be a reasonable assumption. The above described version of the TLTD method does not contain reddening. Therefore, we do not suggest this form of the method for disks with extremely high inclination angles (edge-on orientation). Here, one should perform a correction for reddening before applying the TLTD method. We assumed also that the 10  $\mu\text{m}$  emitting region is smaller, than the outer radius of the disk. If this assumption is not valid, then one has to fit the outer radius as well. Despite these limitations we suggest to use the TLTD method, since the bulk of the young stars with an age of few Myr, where dust processing is thought to be strongest, fit within these criteria.

Although we tested the spectral decomposition methods on spectra of numerous disk models, there are still untested cases. We did not include radial mixing or self-consistent sedimentation in our 2D models and we fixed the input chemical composition in order to investigate the effect of disk structure on the resulting dust composition. These assumptions can have an effect on the resulting chemical compositions of *all* methods. We are aware, that our results were derived from a limited set of input models, based on a common parametrization. However, since we have done the analysis for a number of choices of parameters of the input model, we feel confident that our conclusions are robust. In this paper we presented an efficient method, which can be applied to analyze large data sets in order to obtain a first estimation of the dust composition in the 10  $\mu\text{m}$  emitting region. The main improvement in the TLTD method is the application of a temperature distribution to describe the tem-

perature structure in the disk and the application of multiple continuum components. Since these assumptions are a better description compared to the assumption of the other simpler methods, we think, that the advantage of the TLTD method over the other methods may not be affected by taking into account radial mixing, sedimentation or different chemical compositions.

## 5. Conclusions

Out of the three spectral decomposition methods, tested in this study, the the two-layer temperature distribution (TLTD) method returned dust parameters closest to the input parameters for the calculation of the synthetic spectra. Compared to the results of the TLTD method, the fitted dust composition by the two temperature (TT) method showed larger deviations from the input dust composition, while the results of the single temperature (ST) method deviated even more. Although the mass-averaged grain size estimated by the continuum subtraction (COS) method was very close to the input value in a number of cases, the fitted crystallinity of these models was far away from the 'real' values.

There are several reasons why the previously used spectral decomposition methods have limited capabilities in recovering the dust composition from the  $10\ \mu\text{m}$  silicate feature. The COS method tries to reconstruct a complex continuum by fitting a few data points outside the  $10\ \mu\text{m}$  silicate feature. This can modify the shape of the feature introducing additional uncertainties to the analysis. The ST and TT methods assume, that (i) the source function underlying the emission in the  $10\ \mu\text{m}$  feature can be well approximated by a blackbody curve with a single effective temperature and (ii) the continuum below the feature can also be described by a Planck function with a single temperature. Additionally, there is a degeneracy between optically thin emission of featureless grains (e.g., carbon) and the optically thick emission of the circumstellar disk. Due to this degeneracy, if we included the amorphous carbon into the fit, then the ST method always overestimated the fraction of carbon in the spectra, while the TT method also had this problem in a number of cases. The TLTD suffered less from this problem compared to the other methods due to the more sophisticated estimation of the optically thick emission of the disk.

The exclusion of carbon from the fitted dust species resulted in a better estimation of the total crystallinity in the case of the TT method, although the predicted mass-averaged grain size of the amorphous silicates became too small. For the ST method the exclusion of carbon results in an overestimation of the total crystallinity (up to  $\sim 70\%$ ) even more so than including carbon. Furthermore, the ST method predicted a higher crystallinity for lower stellar luminosities if we excluded the featureless grains from the fit. The mass-

averaged grain size of the amorphous silicates was somewhat larger for the TLTD method without carbon in the fitted dust species.

All the methods overestimated the fraction of large enstatite grains using a wavelength range of 7–14  $\mu\text{m}$ . This behavior is related to the degeneracy of the mass absorption coefficients of large enstatite grains and small olivine, small carbon and medium-sized olivine grains. The overestimation of the large enstatite fraction decreased if we used a broader wavelength range (e.g., 7–17  $\mu\text{m}$ ) for the fit, where the degeneracy is less pronounced.

Although the input dust mixture contained only 4% of large grains (6  $\mu\text{m}$ ) in terms of the total mass mass, the exclusion of this grain population from the fit had an effect on the resulting dust mixture, using a wavelength range of 8–13  $\mu\text{m}$  (ground-based observations). The fitted dust parameters are closer to the input mixture for the COS, ST and TLTD methods if the 6  $\mu\text{m}$  grain population is excluded from the fit. In contrast the TT method returned dust parameters which differed more from the input parameters if we excluded the largest grain population from the fit compared to the results including the 6  $\mu\text{m}$  grains. In the case of the TLTD method, the exclusion of the large grain components modified the mass-averaged grain size of the amorphous dust species. The changes in the estimated fraction of the crystalline dust species, estimated by the TLTD method, are just marginal. In the case of the COS, ST and TT methods the fitted crystallinity was more strongly affected by the exclusion of the 6  $\mu\text{m}$  sized grains. The reason for that was partially that by including large grains in the fit, all methods overestimated the fraction of 6  $\mu\text{m}$  sized enstatite grains.

Here we should note that poorly performing analysis methods can lead to artificial correlations between stellar/disk properties and dust grain parameters. The poor performance of such methods in representing the disk spectral energy distribution is then compensated by introducing emission from non-existing grain components.

The quality of the derived dust parameters depends very strongly on the signal-noise ratio of the observed spectra. For the applied set of optical constants and using a wavelength range of 8–13  $\mu\text{m}$  one can expect an uncertainty of about 11% (in terms of the total silicate mass) in the value of the crystallinity for a S/N of 100. For the same signal-to-noise ration, but using a wavelength interval of 7–17  $\mu\text{m}$  the uncertainty in the value of the crystallinity decreases to 5%. We want to note, however, that probably the higher the crystallinity the easier it is to determine its value regardless of the noise level. This is caused by the sharp peaks of the crystalline material which are easier to identify than the broad feature of the amorphous silicates.

Our tests showed that the optimal wavelength range of the fit is 7–14  $\mu\text{m}$  for the ST and TT method assuming the mass absorption coefficients used in this paper. The width of

this wavelength interval is limited by the similarities in the optical data, which requires the broadest possible interval and the assumption of a single average temperature in the feature and in the continuum, which acts in the opposite direction. The optimal wavelength range for the TLTD method has been found to be 7–17  $\mu\text{m}$ . The application of this broader wavelength range, compared to the simpler methods, resulted in a better estimation of the dust composition. The 7–17  $\mu\text{m}$  interval is broad enough to increase the differences among the mass absorption coefficients. On the other hand, the temperature distribution is a considerably better estimation of the temperature structure compared to an average temperature. Although, the TLTD method provided a better estimation of the dust composition than the other methods, it has been found to be too simple to fit even broader wavelength intervals (e.g., the full *Spitzer* IRS domain, 5–35  $\mu\text{m}$ ). One should therefore use the TLTD method for a first estimation of the dust composition by fitting the 10  $\mu\text{m}$  wavelength range, since a more realistic description of the radial temperature structure and changes in the dust composition is necessary to fit an even broader wavelength range. Another possibility would be to apply the TLTD method for the outer disk (e.g., 20–40  $\mu\text{m}$  interval) and the longer wavelength part of the *Spitzer* spectra and fit this range separately.

On the basis of the results of our study, we propose the following recipe for the analysis the silicate emission features.

1. *Set of mass absorption coefficients.* First, one should investigate how degenerate the fitting problem is, i.e., how the mass absorption coefficients of a given dust species can be reproduced by the linear combination of that of the other dust species. If there are two dust species with very similar mass absorption coefficients, then one should handle them together, since they cannot be distinguished in the fitting procedure<sup>4</sup>.
2. *Global shape of the SED and the disk structure.* The results of our study show that the applied assumption for the temperature structure of the disk is of fundamental importance. Therefore, one should investigate the global shape of the SED of the analyzed source in order to make a reasonable assumption for the disk structure. If the global shape of the SED can be described with a disk model of Chiang & Goldreich (1997), Menshchikov & Henning (1997) or that of Dullemond et al. (2001), then one should use the TLTD method for the analysis of the silicate feature. The TLTD method also has its limitation. In its presented implementation it can handle only disks with a continuous surface density distribution. For instance, if the disk has a large gap in

---

<sup>4</sup>In a real radiative transfer calculation this may be possible since the optical properties of different materials are never completely identical over a large wavelength range.

the region where the silicate emission comes from, then one has to modify the current form of the TLTD method by excluding this temperature range from the fit.

3. *Spectral decomposition with the TLTD method.* Before the TLTD method is applied one has to choose the wavelength range for the fit. We propose a wavelength range of 7–17  $\mu\text{m}$  for space-based observations (with the presented dust model), while for ground based observations the wavelength domain is limited by the Earth’s atmosphere. The continuum should not be subtracted from the spectrum, since this can introduce an additional uncertainty in the results, as our results have shown in the case of the COS method. We suggest to use the TLTD method in the form of integration over temperatures instead of radii in order to avoid assumptions for the outer disk radius.
4. *Interpretation.* The uncertainties in the resulting dust parameters can be estimated by a Monte Carlo type of error estimation from the observational uncertainties. For spectra with low signal-to-noise ratio (few tens) the fitted mass fraction of a single dust component can be very uncertain. Therefore we propose to use robust statistics, like the mass-averaged grain size or the crystallinity, for low S/N data in order to characterize the dust properties. Our test shows that for a S/N of 100 one can expect an uncertainty in the value of the crystallinity of 11 % in terms of the total silicate mass for ground based observations (8–13  $\mu\text{m}$ ). The expected uncertainty for space based observations (7–17  $\mu\text{m}$ ) is 5 % for the same S/N level.

During the interpretation, one also should take into account the systematic errors in the fitting method. Using the optimal wavelength range for the fit, the TLTD method overestimates the mass-averaged grain size of the amorphous silicates by  $50 \pm 30$  %, while the total crystallinity is overestimated by  $8 \pm 7$  %. The increase in the noise level, as well as a narrower wavelength range (8–13  $\mu\text{m}$ ) results in larger mass-average grain sizes for all dust species and higher crystallinity values than the real values.

Th. Henning was supported in part by the National Science Foundation under grant PHY05-51164 (at KITP). We thank an anonymous referee for careful reading the paper and excellent suggestions for improving the text.

## A. Disk models

For the moderately flared and flat disks we use the following density distribution

$$\rho(r, z) = \frac{\Sigma(r)}{H_p(r)\sqrt{2\pi}} \exp\left(-\frac{z^2}{2H_p(r)^2}\right), \quad (\text{A1})$$

where

$$\Sigma(r) = \Sigma_0 \left( \frac{r}{R_{in}} \right)^{-p} \quad (\text{A2})$$

and

$$\frac{H_p(r)}{r} = \frac{H_p(R_{in})}{R_{in}} \cdot \left( \frac{r}{R_{in}} \right)^\alpha. \quad (\text{A3})$$

Here  $H_P$  is the pressure scale height in the disk and  $\alpha$  is the flaring index. For the puffed-up inner rim we applied a similar model than that of Dullemond et al. (2001). However, the scale height of the inner rim was an adjustable parameter. It has been set in such a way, that the shadowed region of the disks relative to their inner radius have to be the same for all models in a given series.

## REFERENCES

- Apai, D., Pascucci, I., Bouwman, J., et al. 2005, *Science*, 310, 834
- Beckwith, S., Henning, T., & Nakagawa, Y. 2000, in *Protostars and Planets IV*, ed. V. Mannings, A. Boss, & S. Russel (University of Arizona Press), 533
- Bouwman, J., Henning, T., Hillenbrand, L., et al. 2008, *ApJ*, (in press), [arXiv:0802.3033]
- Bouwman, J., Meeus, G., de Koter, A., et al. 2001, *A&A*, 375, 950
- Brucato, J., Colangeli, L., Mennella, V., Palumbo, P., & Bussoletti, E. 1999, *Planetary and Space Science*, 47, 773
- Charbonneau, P. 1995, *ApJ*, 101, 309
- Chiang, E. & Goldreich, P. 1997, *ApJ*, 490, 368
- Crovisier, J., Leech, K., Bockelee-Morvan, D., et al. 1997, *Science*, 275, 1904
- Dorschner, J., Begemann, B., Henning, T., Jäger, C., & Mutschke, H. 1995, *A&A*, 300, 503
- Dullemond, C. & Dominik, C. 2004, *A&A*, 417, 159
- Dullemond, C. & Turolla, R. 2000, *A&A*, 360, 1187
- Dullemond, C. P., Dominik, C., & Natta, A. 2001, *ApJ*, 560, 957
- Fabian, D., Jäger, C., Henning, T., Dorschner, J., & Mutschke, H. 2000, *A&A*, 364, 282
- Gail, H.-P. 2001, *A&A*, 378, 192

- Gail, H.-P. 2004, *A&A*, 413, 571
- Harker, D. & Desch, S. 2002, *ApJ*, 565, L109
- Henning, T., Dullemond, C., Wolf, S., & Dominik, C. 2006, *Planet Formation* (Cambridge University Press), 112
- Henning, T. & Mutschke, H. 1997, *A&A*, 327, 743
- Henning, T., Mutschke, H., & Jäger, C. 2005, in *Astrochemistry: Recent Successes and Current Challenges*, ed. L. Dariusz, G. Blake, & E. Herbst (Cambridge University Press), 457
- Honda, M., Kataza, H., Okamoto, Y., et al. 2006, *ApJ*, 646, 1024
- Jäger, C., Molster, F. J., Dorschner, J., et al. 1998, *A&A*, 339, 904
- Kemper, F., Vriend, W., & Tielens, A. 2005, *ApJ*, 633, 534
- Kessler-Silacci, J., Augereau, J., Dullemond, C., et al. 2006, *ApJ*, 639, 275
- Kessler-Silacci, J., Dullemond, C., Augereau, J.-C., et al. 2007, *ApJ*, 659, 680
- Kurucz, R. 1993, in *ASP Conf. Ser. 44, Peculiar Versus Normal Phenomena in A-Type and Related Stars*, ed. M. Dworetzky, F. Castelli, & R. Faraggiana (Astronomical Society of the Pacific), 87
- Lada, C. & Wilking, B. 1984, *ApJ*, 287, 610
- Lawson, C. L. & Hanson, R. J. 1974, *Solving Least Squares Problems* (Prentice-Hall)
- Li, M., Zhao, G., & Li, A. 2004, *ApJ*, 613, L145
- Meeus, G., Sterzik, M., Bouwman, J., & Natta, A. 2003, *A&A*, 409, L25
- Menshchikov, A. & Henning, T. 1997, *A&A*, 318, 879
- Min, M., Hovenier, J., & de Koter, A. 2005a, *A&A*, 432, 909
- Min, M., Hovenier, J., de Koter, A., Waters, L., & Dominik, C. 2005b, *Icarus*, 179, 158
- Min, M., Waters, L., de Koter, A., et al. 2007, *A&A*, 462, 667
- Molster, F. & Waters, L. 2003, in *Astromineralogy*, ed. T. Henning (Springer), 121
- Pascucci, I., Wolf, S., Steinacker, J., et al. 2004, *A&A*, 417, 793



- Pontoppidan, K. & Dullemond, C. 2005, *A&A*, 435, 595
- Preibisch, T., Ossenkopf, V., Yorke, H., & Henning, T. 1993, *A&A*, 279, 577
- Press, W., Teukolsky, S., Vetterling, W., & Flannery, B. 2001, *Numerical Recipes* (2nd ed.) (Cambridge Univ. Press)
- Sargent, B., Forrest, W., D’Alessio, P., et al. 2006, *ApJ*, 645, 395
- Scheegerer, A., Wolf, S., Voshchinnikov, N., Przygodda, F., & Kessler-Silacci, J. 2006, *A&A*, 456, 535
- Servoin, J. L. & Piriou, B. 1973, *phys. stat. sol.*, 55, 677
- Sicilia-Aguilar, A., Hartmann, L., Watson, D., et al. 2007, *ApJ*, 659, 1637
- Taylor, J. 1997, *Error Analysis* (Sausalito: University Science)
- van Boekel, R., Ábrahám, P., Correia, S., & et al. 2006, in *Advances in Stellar Interferometry*, ed. J. Monnier, M. Schller, & W. Danchi, Vol. 6268 (SPIE), 62680
- van Boekel, R., Dullemond, C., & Dominik, C. 2005a, *A&A*, 563, 571
- van Boekel, R., Min, M., Waters, L., et al. 2005b, *A&A*, 437, 189
- Waelkens, C., Waters, L., de Graauw, M., & co authors, . 1996, *A&A*, 315, L245
- Watson, D., Leisenring, J., Furlan, E., et al. 2007, *ApJ*, (in press), [arXiv:0704.1518]
- Wooden, D. 2002, *Earth Moon Planets*, 89, 247

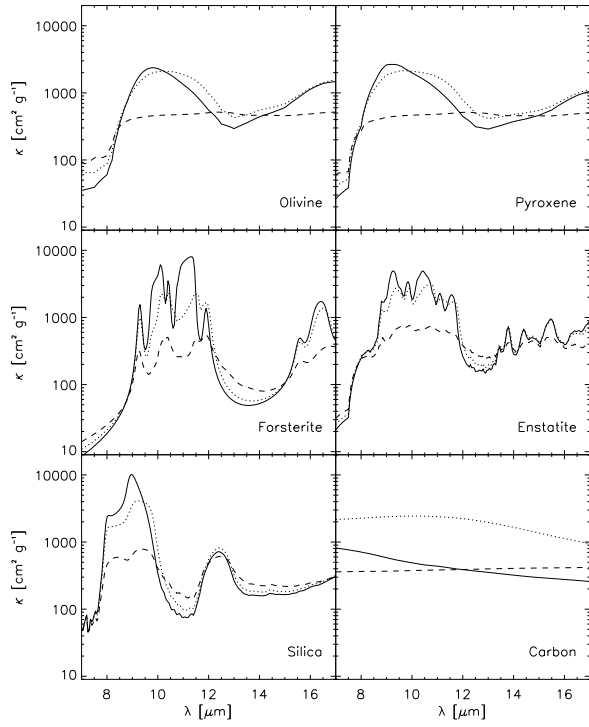


Fig. 1.— Mass absorption coefficients of the dust species used in the tests. All dust species were used with three sizes:  $0.1 \mu\text{m}$  (solid line),  $1.5 \mu\text{m}$  (dotted line),  $6.0 \mu\text{m}$  (dashed line)

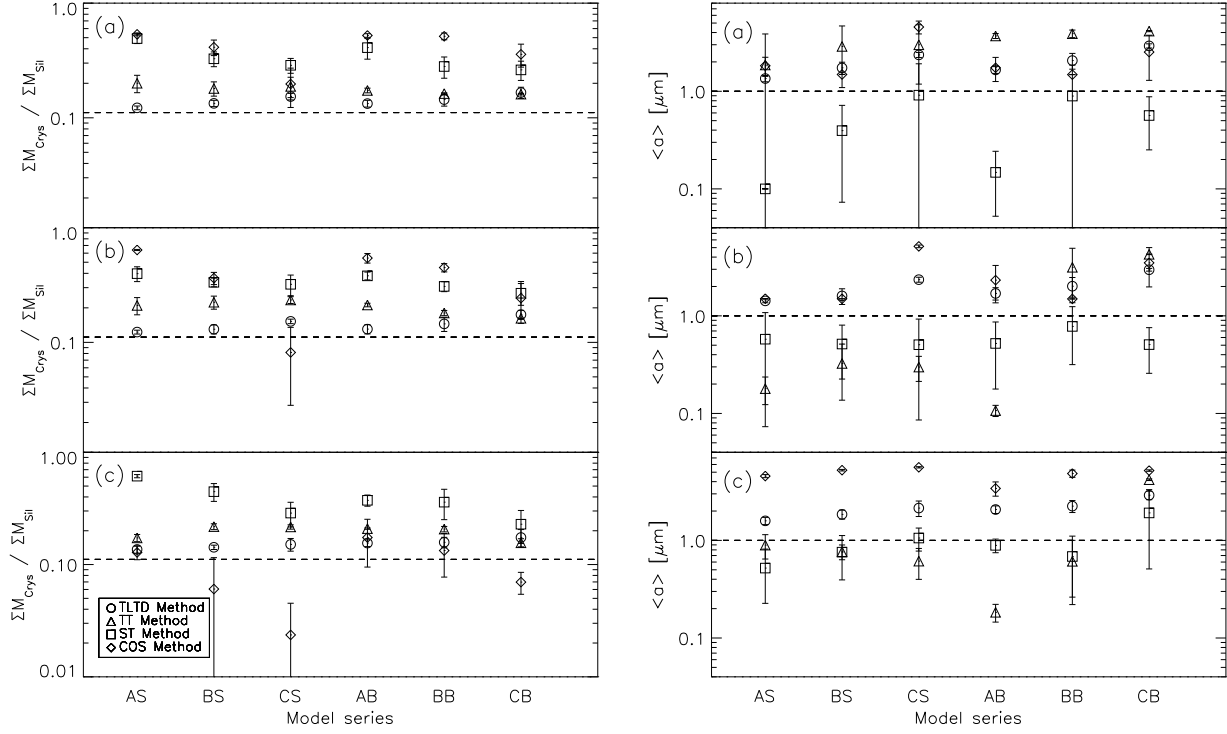


Fig. 2.— Fraction of silicate mass in crystals (*Left*) and mass-averaged grain size (*Right*) for (a) Herbig Ae star, (b) T Tauri star and (c) Brown Dwarf with carbon among the fitted dust species. The symbols show the averaged value over the different inclination angles, and the error bars show the standard deviation. The dashed lines show the input value to the RT code.

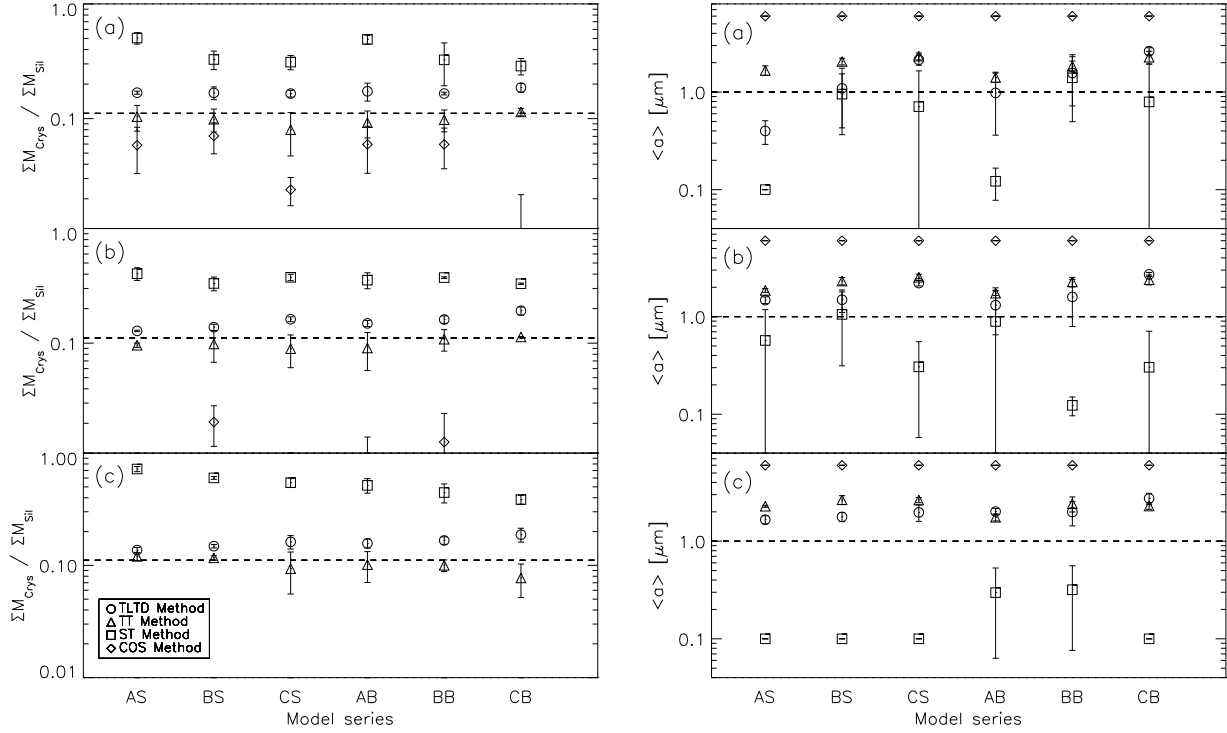


Fig. 3.— Fraction of silicate mass in crystals (*Left*) and mass-averaged grain size (*Right*) for (a) Herbig Ae star, (b) T Tauri star and (c) Brown Dwarf. The spectra were fitted without carbon among the fitted dust species, however carbon is always present in the 2D RT models. The symbols show the averaged value over the different inclination angles, and the error bars show the standard deviation. The dashed lines show the input value to the RT code.

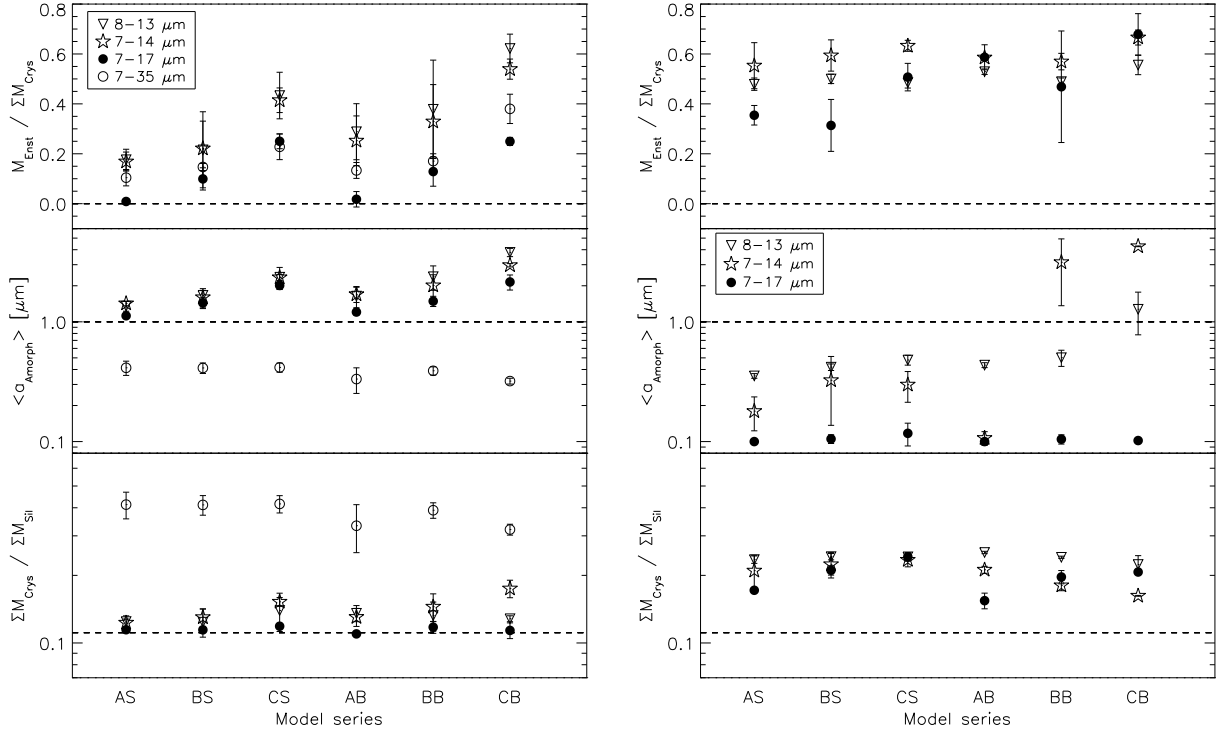


Fig. 4.— The effect of the fitted wavelength range on the results of the T Tauri spectra, fitted by the TLTD method (*Left*) and by the TT method (*Right*). The symbols show the averaged value over the different inclination angles, and the error bars show the standard deviation. The dashed lines show the input value to the RT code.

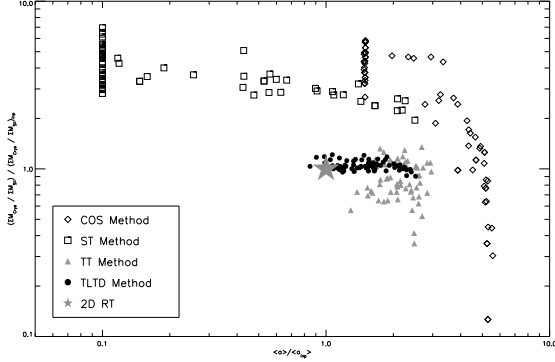


Fig. 5.— Normalized crystallinity as a function of mass-averaged grain size for the best configuration of each method. A wavelength range of  $7\text{--}14\ \mu\text{m}$  was used for the ST, TT and COS methods, while we used  $7\text{--}17\ \mu\text{m}$  for the TLTD method. The spectra were fitted without carbon using the ST and TT methods while for the TLTD and COS methods carbon was included in the fit.

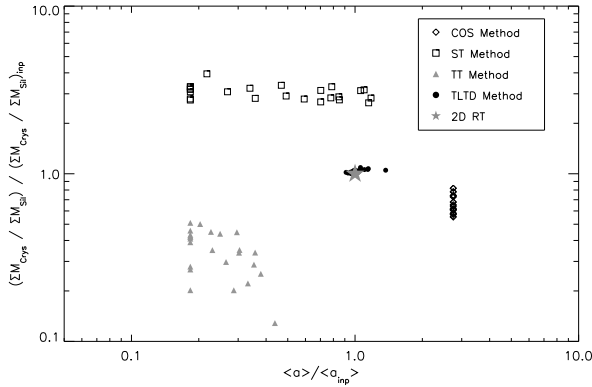


Fig. 6.— Normalized crystallinity as a function of mass-averaged grain size for all T Tauri spectra fitted without  $6\ \mu\text{m}$  size grains. A wavelength range of  $8\text{--}13\ \mu\text{m}$  was used for all methods. Carbon was included in the fit only in the case of the TLTD method.

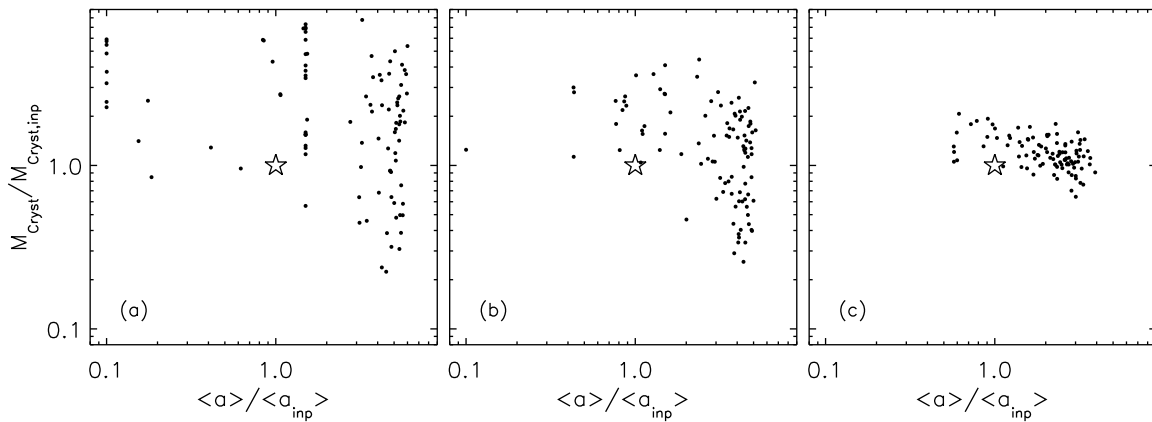


Fig. 7.— Mass-averaged grain size as a function of total crystallinity derived with the TLTD method. Both statistics are normalized to the input value of the 2D RT code (indicated by the star in the middle of the figures). The fitted wavelength range was 8–13  $\mu\text{m}$ , while the applied signal to noise ratios were *a*), 10, *b*) 100, *c*) 1000.

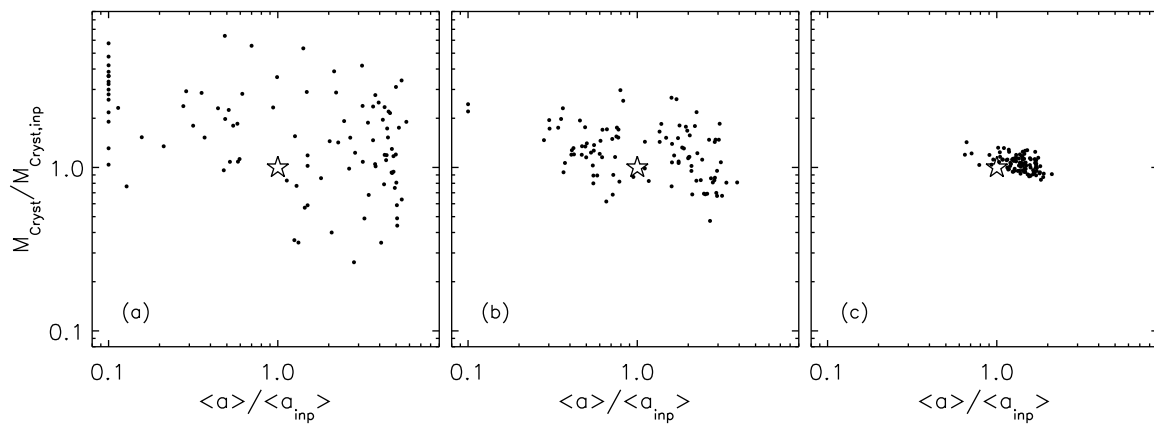


Fig. 8.— Mass-averaged grain size as a function of total crystallinity derived with the TLTD method. Both statistics are normalized to the input value of the 2D RT code (indicated by the star in the middle of the figures). The fitted wavelength range was 7–17  $\mu\text{m}$ , while the applied signal to noise ratios were *a)* 10, *b)* 100, *c)* 1000.



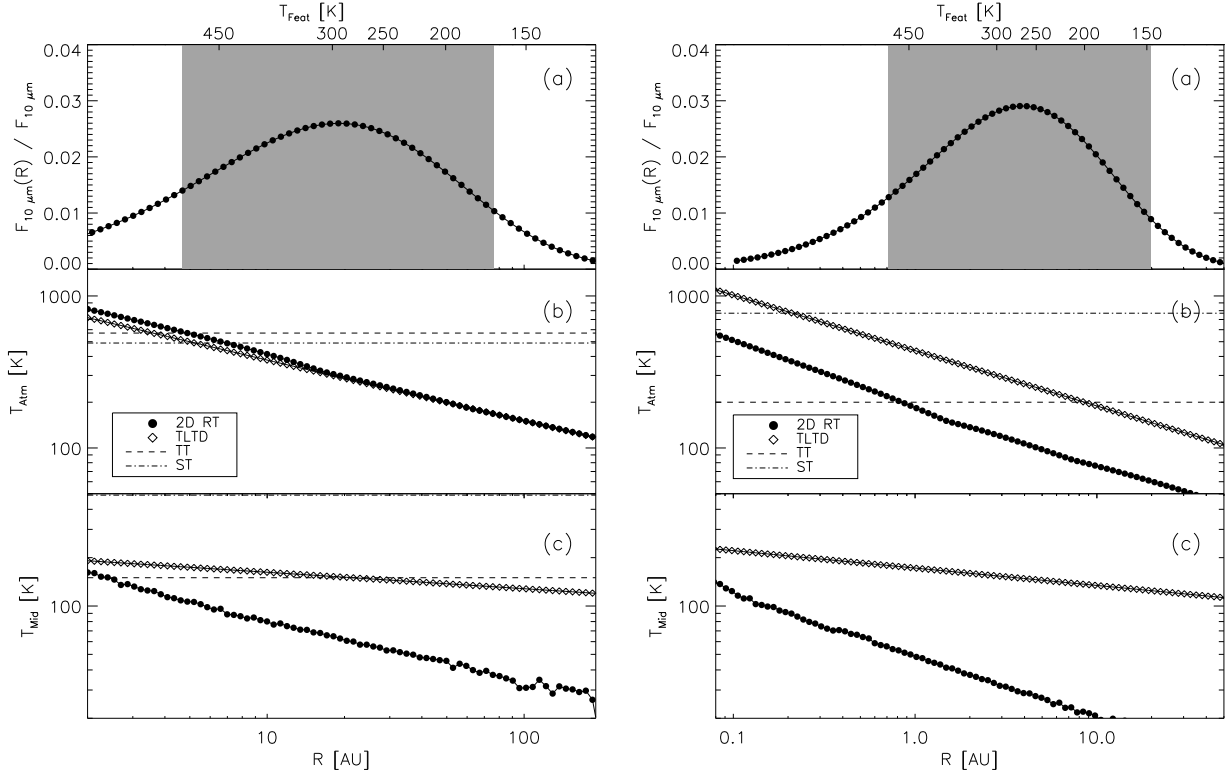


Fig. 9.— (a): Contribution of different annuli to the total flux at 10 μm in the TLTD fit of a Herbig Ae disk model (*Left*) and a Brown Dwarf disk (*Right*) from the BS model series at an inclination angle of 45°. The grey area marks the region from which 70% of the total flux comes from. (b): Radial distribution of the temperature in the disk atmosphere. It has been calculated for the 2D RT model (filled circles), the results of the TLTD code (hollow diamonds), the result of the TT method (dashed line) and the ST method (dot-dashed line). (c): Radial distribution of the temperature in the continuum. The symbols are the same as in the figure in the middle.

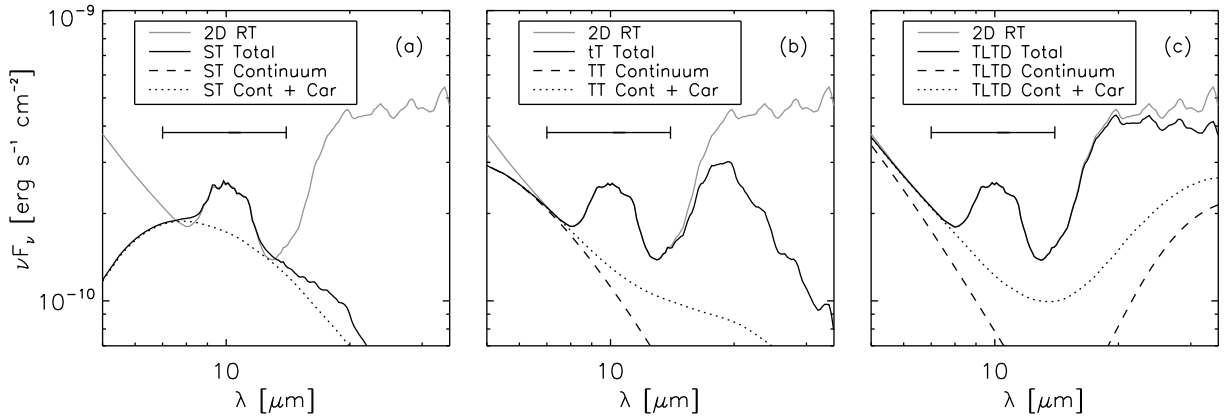


Fig. 10.— Spectrum of a T Tauri model in the AS series at an inclination angle of  $45^\circ$  fitted by *a)* the ST method, *b)* the TT method and *c)* the TLTD method. The horizontal line shows the wavelength range of the fit.

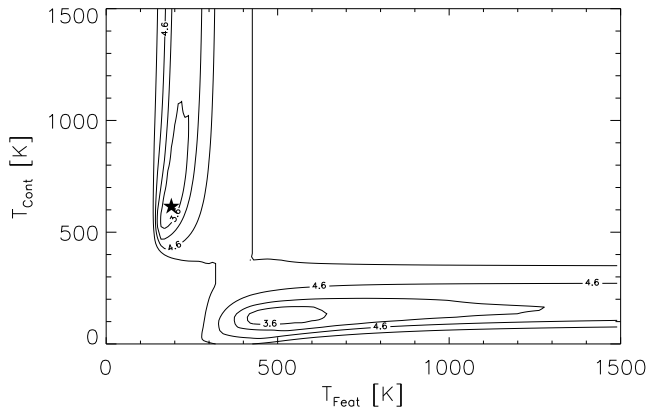


Fig. 11.— Contours of  $\log(\chi^2)$  for the TT method during the fitting of the T Tauri model in the AS series at an inclination angle of  $45^\circ$ . The black star marks the global minimum and the contour lines are separated by 0.5.

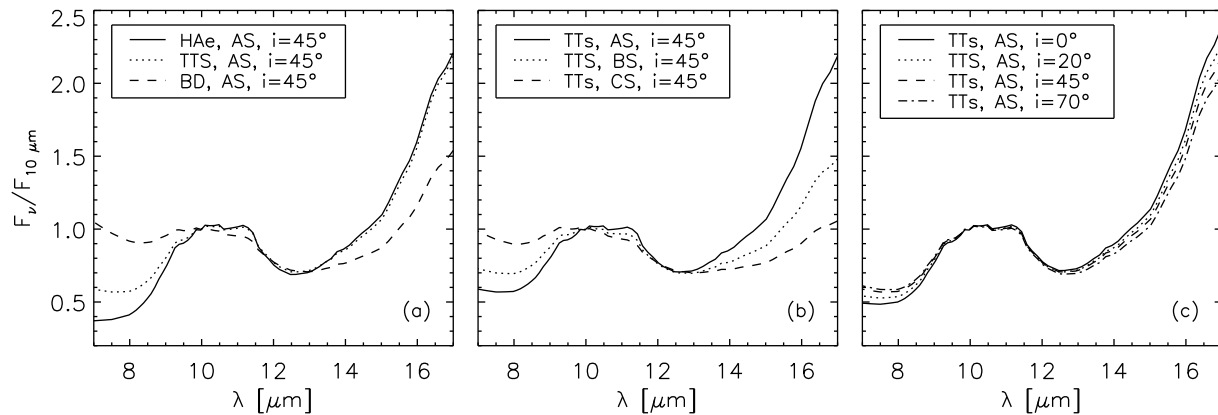


Fig. 12.— Effects of different parameters on the  $10 \mu\text{m}$  features. (a) Spectra of flared disks around different types of stars at an inclination angle of  $45^\circ$ . (b) Spectra of T Tauri stars with different disk geometries (flared, moderately flared and flat) at an inclination angle of  $45^\circ$ . Spectra of T Tauri stars with a flared disk but at different inclination angles.

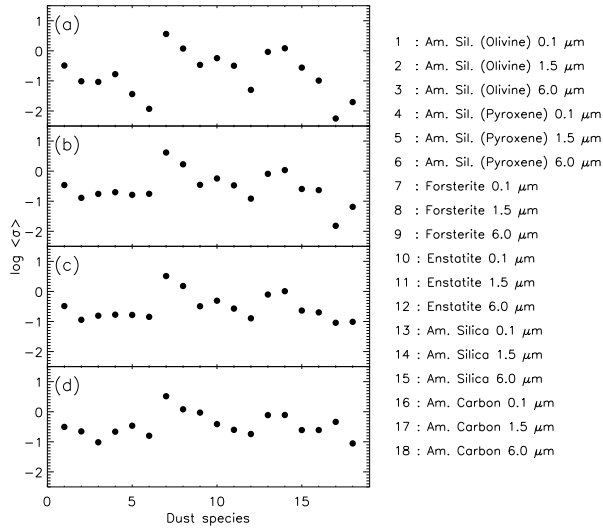


Fig. 13.—  $\sigma$  (for the definition, see Sec.4.4) as a quality indicator of how well the optical data of a specific dust species can be reproduced by the rest. The  $\kappa_{\nu}$  curve of each dust species was fitted using all the other dust species in the wavelength range of (a) 8–13  $\mu\text{m}$ , (b) 7–14  $\mu\text{m}$ , (c) 7–17  $\mu\text{m}$  and (d) 5–35  $\mu\text{m}$  .

Table 1. Main parameters of the 2D RT disk models.

	Herbig Ae star	T Taur star	Brown Dwarf
$L_\star [L_\odot]$	30	1.4	0.035
$T_\star [K]$	9500	4000	2500
$M_\star [M_\odot]$	3	0.55	0.08
$R_{in} [AU]$	0.4	0.087	0.014
$R_{out} [AU]$	400	180	87

Table 2. Overview of dust species used. For each component we specify its lattice structure, chemical composition, shape and reference to the laboratory measurements of the optical constants. For the homogeneous spheres we used Mie theory to calculate the opacities. For the inhomogeneous spheres, we used the distribution of hollow spheres (DHS; Min et al. 2005a), to simulate grain deviating from perfect symmetry.

#	Species	State	Chemical formula	Shape	Ref
1	Amorphous silicate (Olivine stoichiometry)	A	MgFeSiO <sub>4</sub>	Homogeneous sphere	(1)
2	Amorphous silicate (Pyroxene stoichiometry)	A	MgFeSi <sub>2</sub> O <sub>6</sub>	Homogeneous sphere	(1)
3	Forsterite	C	Mg <sub>2</sub> SiO <sub>4</sub>	Hollow sphere	(2)
4	Clino Enstatite	C	MgSiO <sub>3</sub>	Hollow sphere	(3)
5	Silica	A	SiO <sub>2</sub>	Hollow sphere	(4)
6	Amorphous Carbon	A	aC	Homogeneous sphere	(5)

References. — (1) Dorschner et al. (1995); (2) Servoin & Piriou (1973); (3) Jäger et al. (1998); (4) Henning & Mutschke (1997); (5) Preibisch et al. (1993)

Table 3. Result of the spectral decomposition of the spectrum of a Herbig Ae disk with an inclination of  $45^\circ$ . Fitted wavelength domain : 7–14  $\mu\text{m}$ . Similar tables for all fits can be found in the electronic edition of the Journal.

Name	Size [ $\mu\text{m}$ ]	M.Fraction Real [%]	M.fraction COS [%]	M.Fraction ST [%]	M.fraction TT [%]	M.fraction TLTD [%]
Olivine (A)	0.1	15.0	0.0	9.4	14.4	13.5
Olivine (A)	1.5	7.0	19.5	0.0	0.0	6.8
Olivine (A)	6.0	2.0	0.0	0.0	0.0	4.3
Pyroxene (A)	0.1	15.0	0.0	1.5	44.6	14.4
Pyroxene (A)	1.5	7.0	14.8	0.0	0.0	7.4
Pyroxene (A)	6.0	2.0	0.0	0.0	0.0	2.8
Forsterite (C)	0.1	2.0	0.1	1.7	2.5	1.9
Forsterite (C)	1.5	1.0	0.0	0.0	1.4	1.0
Forsterite (C)	6.0	0.0	28.5	0.0	0.0	0.1
Enstatite (C)	0.1	2.0	0.0	1.6	2.6	1.9
Enstatite (C)	1.5	1.0	1.7	2.2	0.1	0.9
Enstatite (C)	6.0	0.0	11.2	3.8	7.6	0.9
Silica (A)	0.1	0.0	0.0	0.0	0.0	0.0
Silica (A)	1.5	0.0	0.0	0.0	0.0	0.0
Silica (A)	6.0	0.0	10.0	0.0	0.0	0.0
Carbon (A)	0.1	46.0	14.0	1.6	0.0	43.8
Carbon (A)	1.5	0.0	0.0	0.0	0.0	0.0
Carbon (A)	6.0	0.0	0.0	78.2	26.7	0.0
Average grain size		1.00	1.5	0.10	0.10	1.35
Total crystallinity		6.00	41.5	9.30	14.20	6.79
T <sub>f</sub> [K]		-	-	380.0	190.0	-
T <sub>c</sub> [K]		-	-	380.0	615.0	-
T <sub>rim</sub> (R <sub>in</sub> ) [K]		-	-	-	-	1408.0
T <sub>atm</sub> (1 AU) [K]		-	-	-	-	755.6
T <sub>mid</sub> (1 AU) [K]		-	-	-	-	171.9
Prim		-	-	-	-	-1.39
Patm		-	-	-	-	-0.35
Pmid		-	-	-	-	-0.10
Reduced $\chi^2$		-	301.6	2697.0	33.19	0.051